

ASSESSING THE IMPACTS OF EXTREME PRECIPITATION AND SEA LEVEL RISE IN  
HANALEI, KAUA‘I THROUGH INTEGRATED COMPOUND FLOOD MODELING

A FINAL REPORT SUBMITTED TO THE DEPARTMENT OF EARTH SCIENCES,  
UNIVERSITY OF HAWAI‘I AT MĀNOA, IN PARTIAL FULFILLMENT OF THE  
REQUIREMENTS FOR THE DEGREE OF

MASTER OF SCIENCE

IN

EARTH AND PLANETARY SCIENCES

August 2024

By

Brian J. Gorberg

Report Committee:

Christopher Shuler, Chairperson

Yinphan Tsang

Abby Frazier

Shellie Habel

Keywords: Flood Model, Compound Flooding, Extreme Precipitation, Sea Level Rise

## **Abstract**

Compound flood events, or the interaction of multiple flood drivers, are expected to become more frequent in Hawai‘i from the combination of sea level rise and more severe flood events and do not consider future flood drivers. Hydrostatic models for sea level rise mapping are available at a high resolution for the Hawaiian Islands, but the methodology does not include flooding from precipitation. There remains a gap in compound flooding research for Hawai‘i. Hanalei, located in northern Kaua‘i, is notable for extreme floods from precipitation and its exposure to passive flooding from sea level rise. Residents at a Hanalei community workshop for climate adaptation highlighted that flooding is the most critical issue to consider out of all climate change issues. To meet this need, a two-dimensional surface water model, the Gridded Surface Subsurface Hydrologic Analysis (GSSHA) model, was created to evaluate compound flooding scenarios in the Hanalei Bay watersheds to bridge the gap.

The model simulates twelve compound flooding scenarios from four extreme precipitation events and three sea level scenarios. The model was calibrated with observed streamflow. Then, the observed streamflow, gauge height, and flood maps were used for validation. The gridded flood depth maps indicated that compound flooding affects primarily the eastern side of Hanalei Bay, specifically the coastal floodplains adjacent to the Hanalei River. The area of compound flooding on the east side of Hanalei Bay is larger than the area determined by hydrostatic models. Still, a higher-resolution surface water and digital elevation model is needed to predict sea level rise inundation more accurately. The flood maps from the model have yet to be recommended for official use, as a higher-resolution topographic dataset with well-documented uncertainty is needed to produce robust simulations that are appropriate for use in planning. Nevertheless, this study provides insight into the development and methodology of compound flood modeling for coastal areas around Hawai‘i.

# Table of Contents

<b>Abstract.....</b>	<b>ii</b>
<b>List of Tables .....</b>	<b>v</b>
<b>List of Figures.....</b>	<b>vi</b>
<b>List of Abbreviations .....</b>	<b>vii</b>
<b>2.0 DATA AND METHODS .....</b>	<b>15</b>
2.1 Model Overview and Data .....	15
2.1.1 GSSHA Model Overview .....	15
2.1.2 Input Data for a Model of Hanalei Bay.....	16
2.1.3 Filling in Missing Rain Gauge Data .....	18
2.1.4 Model Boundaries.....	20
2.1.5 Model Setup for Calibration and Validation .....	21
2.2 Calibration.....	22
2.3 Validation .....	23
2.3.1 Streamflow .....	23
2.2.2 Gauge Height.....	25
2.2.3 Satellite Imagery.....	25
2.3 Parameter Sensitivity.....	26
2.4 Compound Flooding Scenarios .....	28
2.4.1 Extreme Precipitation.....	28
2.4.2 Sea Level.....	30
<b>3.0 RESULTS .....</b>	<b>32</b>
3.1 Calibration.....	32
3.2 Validation .....	33
3.2.1 Streamflow .....	33
3.2.2 Gauge Height.....	34
3.2.3 Satellite Imagery.....	35
3.3 Compound Flood Maps.....	36
<b>4.0 DISCUSSION AND CONCLUSIONS .....</b>	<b>40</b>
4.1 Uncertainties and Limitations .....	40
4.1.1 Enhancing Calibration Methods for Improved Flood Predictions .....	40

4.1.2 <i>Enhancing the Gauge Height Validation</i> .....	41
4.1.3 <i>Rain Gauge Interpolation and its Effect on Streamflow Validation</i> .....	41
4.1.4 <i>Discrepancies Between the Satellite Imagery and Modeled Flood Maps</i> .....	42
4.2 Effects of DEM Resolution on Sea Level Rise Inundation in the GSSHA Model .....	43
4.3 Improved Risk Assessment and Mitigation Through Compound Flood Models .....	44
4.4 Future Directions for Enhancing Compound Flood Modeling in Hanalei.....	45
<b>Appendices</b> .....	<b>48</b>
Appendix A: Duration and Total Number of Floods .....	48
Appendix B: Python Scripts .....	48
Appendix C: Download Link for the GSSHA model of Hanalei Bay .....	48
Appendix D: Manning’s n Roughness Coefficients.....	49
Appendix E: Metadata of Stream and Rain Gauges.....	50
Appendix F: Infiltration Parameters.....	51
Appendix G: Damage Report of Each Gauge Height Event.....	52
Appendix H: USGS 16103000 Stream Gauge’s Streamflow Return Periods.....	53
Appendix I: NSE Values from Calibration Simulations .....	53
Appendix J: Graphs of Validation and Calibration Simulations.....	54
Appendix K: Compound Flood Maps .....	55
<b>References</b> .....	<b>56</b>

## List of Tables

Table 1: GSSHA input data for Hanalei Bay .....	17
Table 2: Extreme precipitation events used for calibration and validation .....	22
Table 3: Acceptable values for validation statistics.....	25
Table 4: GSSHA Input data for infiltration parameterization .....	27
Table 5: Gauge height scenarios .....	29
Table 6: Sea level scenarios .....	30
Table 7: Average NSE values from calibration .....	32
Table 8: Performance statistics for the streamflow validation.....	34
Table 9: Calibrated Manning’s n roughness coefficients .....	49
Table 10: Metadata for the stream and rain gauges used in GSSHA.....	50
Table 11: Soil Parameter values for Green and Ampt single layer infiltration .....	51
Table 12: Soil layer hydraulic conductivity and thickness for multi-layer infiltration.....	52
Table 13: Damage report for the gauge height events .....	52
Table 14: Streamflow return periods .....	53
Table 15: NSE values for each calibration simulation.....	53

## List of Figures

Figure 1: Duration and total number of flood events around Kauai .....	10
Figure 2: Images of flooding in Hanalei .....	11
Figure 3: Land uses and watersheds of Hanalei Bay .....	14
Figure 4: Filling in missing rain gauge data .....	19
Figure 5: GSSHA model boundaries and gauges .....	21
Figure 6: Infiltration parameter sensitivity .....	28
Figure 7: Hydrographs of the gauge height scenarios .....	29
Figure 8: Water level data from the Nawiliwili buoy .....	31
Figure 9: NSE values from calibration simulations .....	33
Figure 10: Observed vs. modeled streamflow of a validation simulation .....	34
Figure 11: Observed vs. modeled gauge height.....	35
Figure 12: Observed and modeled flood maps .....	36
Figure 13: Number of parcels flooded for each compound flooding scenario .....	37
Figure 14: Areas of increased inundation from sea level rise.....	38
Figure 15: Comparing hydrostatic models and compound flooding results .....	38
Figure 16: Observed vs modeled streamflow for all simulations .....	54
Figure 17: All compound flood maps .....	55

## **List of Abbreviations**

1. 3DEP: 3D Elevation Program
2. C-CAP: Coastal Change Analysis Program
3. DEM: Digital Elevation Model
4. FEMA: Federal Emergency Management Agency
5. GSSHA: Gridded Surface Subsurface Hydrologic Analysis
6. KGE: Kling-Gupta Efficiency
7. NCEI: National Center of Environmental Information
8. NOAA: National Oceanic and Atmospheric Administration
9. NSE: Nash Sutcliffe Efficiency
10. PBIAS: Percent Bias
11. USACE: United States Army Corps of Engineers
12. USDA: United States Department of Agriculture
13. USGS: United States Geological Survey
14. WMS: Watershed Modeling Software

## 1.0 INTRODUCTION

Coastal communities in Hawai‘i often experience floods from high sea levels (Thompson et al., 2019) and extreme precipitation events (Huang et al., 2021). The steep watersheds, highly impermeable soils, and intensity of precipitation events expose the coastal communities to extreme flooding (Fares, 2008; Shade, 1996). Also, the relatively flat topography of these coastal communities exposes them to chronic flooding from sea level rise. Sea level rise can accelerate flooding along the coastline and increase the magnitude of extreme precipitation flood events. However, changes in the sea level and extreme precipitation patterns can augment flood potential and increase the frequency of compound events (Wahl et al., 2015). When multiple flood drivers interact, they cause a compound flood event. The flooding from a compound event is much greater than just one flood driver. Estimating compound flooding through modeling and mapping methods improves flood mitigation projects, enhances the risk assessment for planners, and prepares the community for changes in flooding.

The magnitude and frequency of compound flooding events will likely increase because of sea level rise and changes in extreme precipitation patterns (AghaKouchak et al., 2020). Global models show that extreme precipitation intensity is expected to increase by at least 50% by the end of the century under the SSP5-8.5 no-mitigation scenario (Chen and Sun, 2021). Thackeray et al. (2022) also found a 32% to 55% increase in the occurrence of global extreme precipitation events at the end of the century. Researchers in Hawai‘i are already observing increasing trends in extreme precipitation recorded at rain gauges (Gayte et al., 2022). The number of minor flood events from high sea level in Hawai‘i is projected to increase from just 0.2 events per year in 2020 to 9 events annually by 2050 (Sweet et al., 2022). The minor floods from sea level rise increase the chances of an extreme precipitation event co-occurring with a higher sea level. The Hawai‘i State Climate Commission estimates that 6,500 shoreline structures around the islands of Hawai‘i could be damaged from 3.2 feet of sea level rise alone (Laramee et al., 2022). The actual damage of sea level rise will be higher than expected when extreme precipitation is considered in the analysis. Compound flood models can estimate the extent of inundation from the interaction of a higher sea level and an extreme precipitation event.

Baseline hydrologic and hydrostatic models estimate extreme precipitation events or sea level rise floods, but a gap remains in the number of Hawai‘i models that simulate the combination of the two. Baseline hydrologic models, such as the models for the Federal

Emergency Management Agency (FEMA) Flood Insurance Rate Maps, estimate flooding from historical extreme precipitation events (FEMA, 2010) and often do not account for compound flooding from storm surges, sea level rise, or projected changes in extreme precipitation. Hydrostatic models estimate sea level rise inundation using the assumption that flooding is based solely on ground elevation relative to sea level. The methodology for the hydrostatic models in Hawai‘i does not include flooding from precipitation (Anderson et al., 2018). Hydrologic models should incorporate compound flood drivers to enhance flood management planning and mitigation projects in coastal regions of Hawai‘i that are highly exposed (Xu et al., 2023). Unlike hydrostatic models, compound flood models are more data-intensive and require much more computational time. For this reason, new compound flood models need to be assessed in Hawai‘i one region at a time to address specific flooding issues for each watershed. There should also be a focus on scaling compound flood models so that the agendas of county or statewide planners can progress.

Accurately estimating the spatial extent of compound flood characteristics like depth is best achieved through dynamic numerical flood models. Other techniques, such as risk mapping and statistical models, can be used to assess the risk of compound events. Sun et al. (2024) found compound flooding to be an ever-growing area of study, with the number of related annual publications increasing from 9 per year in 2014 to 85 per year in 2022. Sun et al. (2024) also pointed out that 2D or 3D numerical models are the best predictors for flood extent as they consider an area’s physical details and fluid dynamics. Modeling methods should be tailored to the specific geographic attributes of a study region. Future compound flood models should consider the uncertainties of different models and the impact of climate change on extreme precipitation events and sea levels (Xu et al., 2023). Compound flood models, independent from the maps made for insurance, are crucial for improving resilience as they help management identify coastal areas with hidden risks (Mitu et al., 2023).

Although every island experiences severe flood events, Kaua‘i’s history of flooding and progressive flood management plans make it a good starting point for compound flood modeling. Its round shape, moderate summit elevation, and northernmost location make extreme precipitation events more frequent and intense than other Hawaiian Islands (Chu et al., 2009). The planners and residents are well aware of these flooding issues. On October 5th, 2022, Kaua‘i County Council unanimously approved Bill No. 2879 to become one of the first counties in the

nation to regulate development in areas exposed to sea level rise. A community workshop held by the County of Kaua‘i Planning Department in 2022 showed residents generally agreed that sea level rise, extreme precipitation, and tropical cyclones are the most critical issues to consider when planning for climate change (Kaua‘i Climate Adaptation Plan, 2022). Compound flood models and extreme precipitation projections can be used to enhance the tools used by County planners. FEMA flood maps limit the County planners’ ability to plan for compound flood events. Hanalei, located on the northern side of Kaua‘i (Figure 1), is a focus point of flooding issues for residents and county planners.

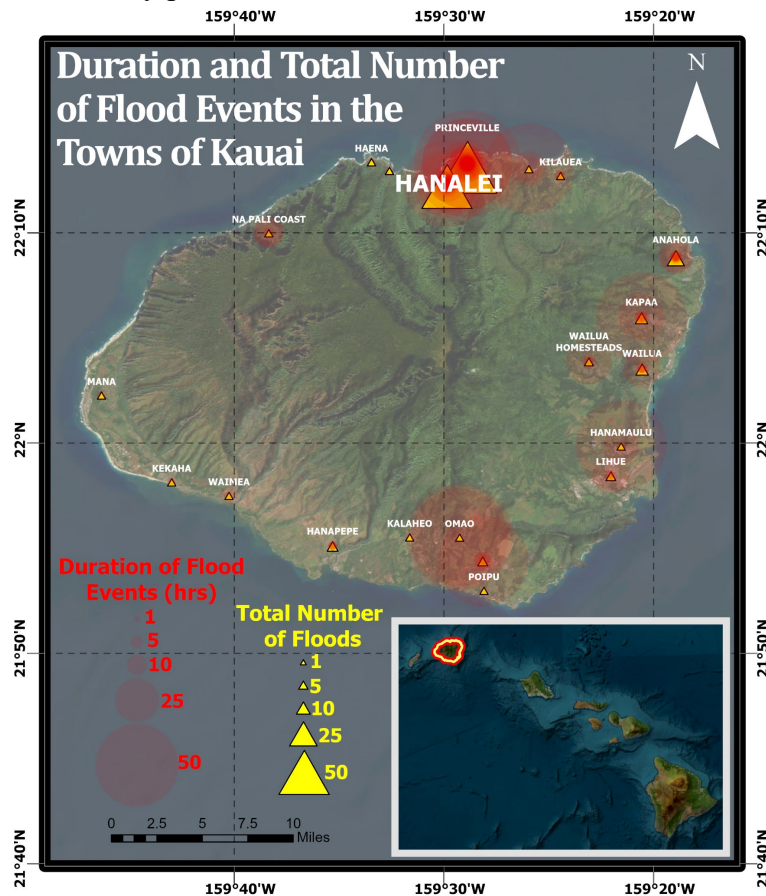


**Figure 1:** The duration and total number of flood events around Kaua‘i are shown in this map (NCEI, 2022). The link to download the shapefiles can be found in Appendix A.

Hanalei is more exposed to extreme precipitation and rising sea levels than other towns in Kaua‘i. Bezore (2014) used a hydrostatic model to show that Hanalei had a higher percentage of sea level rise inundation than other nearby towns. Storm event data between 1996 and 2022 (NCEI, 2022) showed Hanalei had the longest-lasting and most significant number of flood

events (Figure 1). Although research suggests there is an overall decline in precipitation across the islands of Hawai‘i (Frazier and Giambelluca, 2017), Gayte et al. (2022) found that Hanalei and other northern towns in Kaua‘i exhibit a positive trend in extreme precipitation events, precisely the 100-year return period for six-hour precipitation accumulations. Understanding extreme precipitation projections may be necessary for adequate estimations of events that may occur when sea level rise becomes more apparent at the end of the century.

The extreme precipitation event of April 2018 is a display of the magnitude of flooding that can occur in Hanalei (Figure 2). This event broke the United States’ 24-hour precipitation accumulation record. Nearly 50 inches of precipitation accumulated within 24 hours at a rain gauge at the Waipā Garden, located within Hanalei Bay just north of Mount Wai‘ale‘ale (Corrigan and Businger, 2022). Around 532 homes were damaged, causing 19.7 million USD in losses (NCEI, 2022). Residents and county planners have concern that extreme precipitation events, like the event of April 2018, may intensify or become more frequent. For these reasons, the watersheds of Hanalei became the focus of compound flood modeling.



**Figure 2:** These pictures show the extent of flooding in Hanalei during extreme floods. The sources for the images include the right photo by Taylor (2018) and the left photo by Mathews (2018).

Hanalei's floods impact local agriculture, critical habitats, and transportation. Hanalei Bay is a popular tourist destination and a vital source of local agriculture, fishing, and cultural heritage. Hanalei Bay supports surfing, boating, fishing, and other recreational activities (Pettersen et al., 2012). Sedimentation from floods hinders boating access between the Hanalei River and the ocean and degrades the critical habitat for endangered species (Field et al., 2007). Hanalei Valley is characterized by pond-like structures that hold water and facilitate the growth

of kalo (taro; *Colocasia esculenta*), the plant from which poi is made. Extensive quantities of taro are sold on the commercial market, and some taro is grown and consumed as part of the local diet (Pettersen et al., 2012). Agriculture in Hanalei was established in the region as early as the 7th century A.D (Schilt, 1980). Sedimentation and pollution from extreme flood events can disrupt taro production and harm the industry. The Hanalei Bridge (east side of Hanalei Bay) is the only way to get into or out of the town and often closes multiple times a year because of flooded roadways. Other bridges on the west side of Hanalei Bay have also closed because of flooding or debris. Hanalei's isolation makes it difficult to support tourists trapped within Hanalei from bridge closures. The bridge closure also makes it difficult for residents to leave or enter Hanalei to reach their homes or emergency services. Flood models can improve the community's resilience to extreme compound flood events.

Most existing surface water models for Hanalei do not account for compound flooding from high sea levels and extreme precipitation; descriptions of these models are provided below. Fares et al. (2014) evaluated the performance of the National Weather Service model, the Hydrology Laboratory Research Distributed Hydrologic Model (HL-RDHM), in simulating the hydrology of the Hanalei watershed. Although this model cannot reveal flood extent, duration, and depth, the discharges from the HL-RDHM could provide input data for hydraulic modeling. Other models were made to evaluate the sediment and pollutant loads for Hanalei Bay. Fuddy & Abercrombie (2011) used the Environmental Fluids Dynamic Code to model the hydrodynamic and water quality of Hanalei Bay while using the Loading Simulation Program in C++ to model the hydrology and pollutant accumulation/wash-off. Hagedorn and El-Kadi (2009) used the FLO-2D flood routing model to estimate runoff and suspended sediment fluxes. FLO-2D can model flood extent and depth, but the model made by Hagedorn and El-Kadi (2009) does not have that purpose. Cheng et al. (2007) compared the Nonpoint Source Pollution Erosion Comparison model and the Annualized Agricultural Nonpoint Source Pollution model to evaluate the runoff and erosion in Hanalei. The Sustainable Resources Group International Inc. (HWH and SRGI, 2023) evaluated flood mitigation strategies using a model that combined extreme streamflow and sea level rise. Their modeling focused on changes in stream depths and did not incorporate gridded flood maps in their results. Also, their model included only half of the watersheds draining into Hanalei Bay. Flood models in Hanalei Bay will show increased

inundation if multiple flood drivers are included (Sangsefidi et al., 2023). There remains a gap in 2-D compound flood inundation models for Hanalei, Kaua‘i.

The Gridded Surface Subsurface Hydrologic Analysis (GSSHA) model could be used to simulate compound flooding scenarios in the watersheds of Hanalei Bay and provide gridded flood depth maps. GSSHA is widely used by hydrologic modelers for flood inundation modeling (Afshari et al., 2016; Pradhan et al., 2019) as the model meets the minimum requirements of the National Flood Insurance Program in the United States (FEMA, 2022). The model is often used to assess compound flooding (Pradhan et al., 2019). GSSHA has also been used to model diverse watersheds, ranging from coastal urban areas (Brendel et al., 2021) to tropical volcanic islands (Ogden, 2016; Manrique et al., 2021). GSSHA could simulate extreme precipitation and sea level rise in Hanalei Bay (Downer and Ogden, 2006). GSSHA’s widely accessible input data in Hawai‘i allows GSSHA to be scalable to many other watersheds outside Hanalei Bay. The small grid size option in GSSHA enables the model to produce high-resolution flood maps. GSSHA runs at time steps as small as one second or as high as one hour, making it appropriate for extreme precipitation simulations. Its high spatial and temporal resolution makes GSSHA suitable for the watersheds of Hanalei Bay.

The four main watersheds that drain into Hanalei Bay (Waikoko, Waipā, Wai‘oli, and Hanalei) are located on the northern side of Kaua‘i, extending from the island's center to the coastline (Figure 3). The watersheds’ topography varies from steep mountainous regions to flat valley floodplains, contributing to diverse hydrological processes. Most of the land in the watersheds is undeveloped and classified as ‘Evergreen Forest’ land use (NOAA C-CAP, 2010). The Hanalei watershed is the largest of the four, and the Hanalei River contributes the most significant flooding to the town. The river originates from Mount Waialeale, one of the wettest spots on Earth, and flows through the Hanalei Valley before emptying into the bay. The tides in Hanalei Bay affect roughly one mile of the Wai‘oli Stream and nearly three miles of the Hanalei River (HWH and SRGI, 2023). These four watersheds represent the boundary for the model.

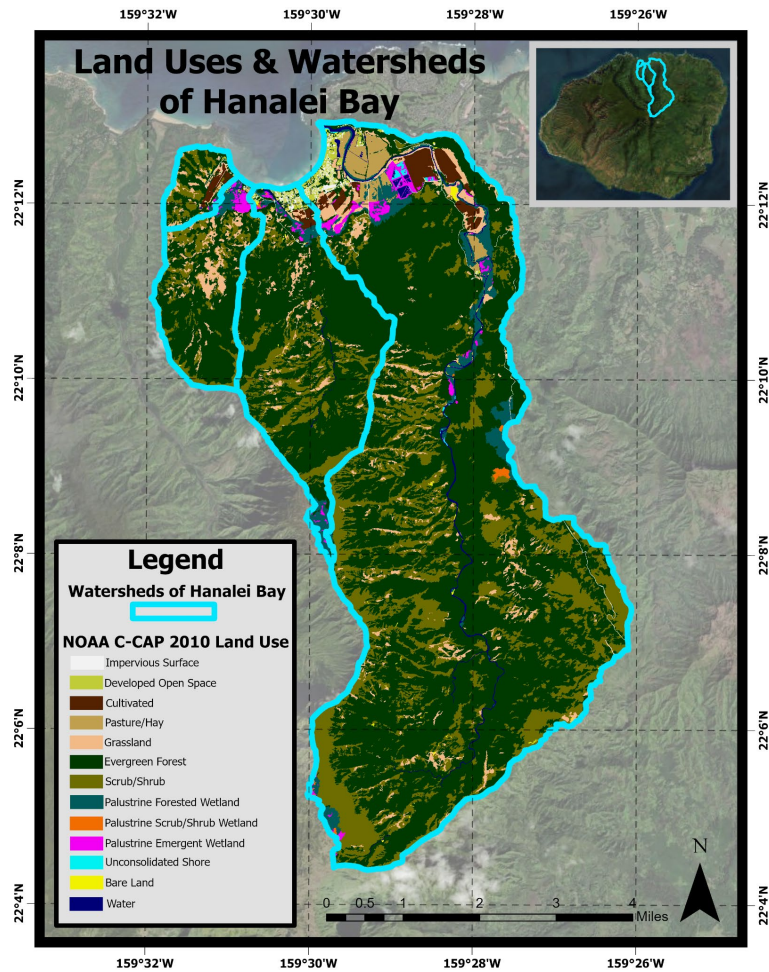


**Figure 3:** This map shows the four watersheds (Hawai'i DLNR DAR, 2020) and the land use map (NOAA C-CAP, 2010) used for the model.

This research aimed to evaluate compound flooding simulations using a GSSHA model of the watersheds that drain into Hanalei Bay. To do this, a new GSSHA model was created using the calibration and validation methods widely accepted by hydrologic modelers. Compound flooding scenarios were explored in various simulations to produce detailed flood inundation maps. When extreme precipitation events in Hanalei interact with a higher sea level, the flooding should be more significant than expected from just extreme precipitation alone (Hendry et al., 2023). A higher sea level produces a higher downstream water height boundary condition in a river's estuary, causing the water to back up and increase the flood depths further upstream (Garcia and Loaciga, 2013). The modeling helps identify areas of Hanalei Bay subject to compound flooding. The model methodology and modeling results are evaluated for their effectiveness in planning and scalability to other watersheds.

## 2.0 DATA AND METHODS

### 2.1 Model Overview and Data

#### 2.1.1 GSSHA Model Overview

GSSHA models use various hydrologic processes (infiltration, sea level, vegetation interception, evapotranspiration, groundwater, snow melt, etc.) to model flooding. For this study, the four main watersheds that drain into Hanalei Bay (Waikoko, Waipā, Wai‘oli, and Hanalei) were included in the model. The location of these watersheds and the land uses can be found in Figure 3. By including all of these watersheds, the compound flooding effects of sea level rise and extreme precipitation could be explored throughout all communities of Hanalei Bay. Also, previous surface water models for Hanalei primarily focused on the Hanalei and Wai‘oli watersheds instead of including Waipā and Waikoko. GSSHA implements Hortonian flow as the dominant runoff mechanism (Downer and Ogden, 2006). Groundwater, infiltration, and subsurface preferential flow processes contribute a negligible difference in runoff during extreme events. Since most runoff in Hanalei occurs from excess precipitation rather than elevated groundwater levels, Hortonian overland flow was determined to be the dominant runoff mechanism (Wahlstrom et al., 1999). Ogden (2016) also applied GSSHA to the watersheds on the tropical island of Dominica. The watersheds Ogden (2016) evaluated have characteristics similar to those of Hanalei Bay. Ogden found that it is not uncommon for tropical volcanic watersheds to have nearly all precipitation turn into runoff during an intense event. Further analysis of the model outputs for Hanalei indicated which processes needed to be included.

The input data for the parameterization of hydrologic processes in GSSHA is widely accessible for Hawai‘i, making GSSHA scalable to many watersheds outside of Hanalei Bay. The hydrologic processes for GSSHA models are often limited by the uncertainty in parameterization (Costabile et al., 2020; Mirchi et al., 2009). A more complex model that uses many hydrologic components, such as groundwater and infiltration, does not always produce an accurate output (Downer and Ogden, 2006). A model with groundwater baseflow will provide a precise estimation of streamflow during low streamflow events, but this hydrologic process is practically negligible during high streamflow events. It would be necessary to use groundwater parameterization if the goal of this study was to model streamflow during drier months when the

stream is fed almost entirely by groundwater baseflow. Since high streamflow events are the priority for flood modeling, groundwater parameterization is unnecessary to achieve approvable streamflow validation for higher streamflow events. The final model was set up as a ‘concrete’ model, meaning infiltration processes were omitted. The initial setup evaluated two different infiltration processes to determine if infiltration was necessary for the final calibrated model. Section 2.3 goes into more detail about the infiltration parameterization and its effect on the model’s performance.

### *2.1.2 Input Data for a Model of Hanalei Bay*

The data sources for the model included maps, parameter values from literature or databases, and various rain (9) and stream (2) gauges. The Python Scripts and additional data used to build the model can be downloaded from the link found in Appendix B. The final model can also be accessed through the link in Appendix C. The sources of the data, their resolution, and usage within the final model are shown in Table 1. New data sources, such as a topographic dataset from a recent flood mitigation study in Hanalei (HWH and SRGI, 2023), will likely become available, and the model may need to be updated soon. Higher-resolution topographic data may improve the model’s performance.

**Table 1:** This table contains the data for setting up the initial parameters of the model. The sources and resolution of each data are also shown.

GSSHA Model Parameter	Data	Resolution	Source
<i>GSSHA Maps</i>			
Topography Map	USGS Digital Elevation Model	10 m	USGS (2013)
Land Use Map	NOAA C-CAP (2010) Land Use Land Cover	10 m	NOAA C-CAP (2010)
<i>Rain Gauge and Stream Gauge Data</i>			
Precipitation	rain gauges and radar	hourly	Huang et al. (2022)
Monthly precipitation for filling in missing rain gauge data	Mean monthly precipitation raster maps	monthly	Giambelluca et al. (2013)
Streamflow	USGS stream gauges (16103000 and 16104200)	hourly	USGS National Water Information System
<i>Roughness Parameterization</i>			
Manning's n roughness coefficients for the land use map	Table of NOAA C-CAP (2010) land use and roughness value		Roughness coefficients from Mattocks and Forbes (2008). Visual validation by USACE (2020) for a watershed on O'ahu.

The uncertainty and vertical resolution values for the digital elevation model (DEM) input data is unavailable. The DEM used for the model was obtained from USGS (2013) and had a horizontal grid size resolution of one-third Arcsecond, roughly equivalent to 10 meters. This DEM was outside USGS's current 3D Elevation Program (3DEP) lidar collection area and is an old version of the legacy National Elevation Dataset. The data for the DEM was derived in 1999 from surveyed contour data on historical maps dating from 1960. The DEM was republished under 3DEP in 2013. Some of the product-specific information for the DEM has been lost, so the uncertainty and vertical resolution of the DEM could not be determined by the metadata. The 3DEP subject matter experts at USGS could not figure out the uncertainty and vertical resolution of this DEM either. The Watershed Modeling Software (WMS) automatically manipulated the DEM to reduce damming and promote flow. This DEM manipulation method was only used for models with a grid size larger than 10 meters.

The coastal boundary for the model was determined using the zero-meter contour of the DEM used in the model. A continuous time series of tidal data was not used at the coastal boundary. Instead, a constant stage height was applied to the boundary throughout each

simulation. If the watery height at the boundary is high enough, the nearest grid cells will overtop with water, and the inundation will propagate forward. This water can back up and interact with the streamflow. The constant stage height was increased to simulate the sea level rise scenarios.

GSSHA requires a land use map to define the values for the Manning's  $n$  roughness parameters. The NOAA C-CAP (2010) map of Hanalei was used for roughness parameterization. The Manning's  $n$  roughness coefficients USACE (2020) provided for each NOAA C-CAP land use were used for the initial parameterization. USACE (2020) used these parameters for a watershed model on O'ahu and visually inspected the land use to validate the Manning's  $n$  roughness value. The Manning's  $n$  roughness coefficients for the calibrated model can be found in Table 9 of Appendix D.

GSSHA interpolated the precipitation using inverse distance weighting in each simulation. The model's simulations used rain gauges distributed around the model boundaries to simulate precipitation. GSSHA required the rain gauge data to have one-hour or less time increments. Huang et al. (2022) provided the hourly rain gauge and radar data. Some rain gauges or radar data did not report representative precipitation during events due to heterogeneity in the precipitation distribution or gauge/signal malfunctions. Thus, nonrepresentative rain gauge data was omitted to ensure an accurate precipitation interpolation in each simulation. GSSHA requires a complete dataset for each rain gauge. The methodology to fill in the missing rain gauge data is described in the next section.

### *2.1.3 Filling in Missing Rain Gauge Data*

Various statistical methods can be used to fill in the missing rain gauge data. The normal ratio method is one equation (Equation 1) that is often used. Cheng et al. (2007) used the normal ratio method to fill in missing rain gauge data for a surface water model of Hanalei. It requires using at least three nearby rain gauges and the average monthly precipitation of each rain gauge. Giambelluca et al. (2013) provide average monthly precipitation maps of Hawai'i. This method works best when the missing data is before or after the peak of the precipitation event so that the precipitation recorded during the event is mostly accurate (Nadiatul Adilah and Hannani, 2021). Figure 4 shows an example of applying the Normal Ratio Method to fill in missing data at the Hanalei rain gauge (SKN: 1117.8).

The hourly radar data acquired from Huang et al. (2022) was used to fill in the missing rain gauge data when applicable. Not all of the rain gauges are covered by the radar data extent. Also, the radar data only extends from the start of 2016 to the end of 2021. If a rain gauge was in a region where radar data was available, the missing rain gauge data was filled in using the radar data. One thing to note was the radar data was sometimes unreliable for certain extreme precipitation events. Since Hanalei has poor radar coverage, it is possible for some of the precipitation data to be missing or inaccurate for some events. Radar was only used if the radar showed similar precipitation patterns as nearby rain gauges.

**Equation 1:** This is the normal ratio method equation and was taken from Nadiatul Adilah and Hannani (2021).

$$p_x = \frac{1}{m} \sum_{i=1}^m \left( \frac{N_x}{N_i} \right) p_i$$

$N_x$  = Normal annual precipitation of the X station

$p_x$  = Estimate for the target station (X)

$p_i$  = Rainfall values of rain gauges used for estimation

$m$  = Number of surrounding stations

15

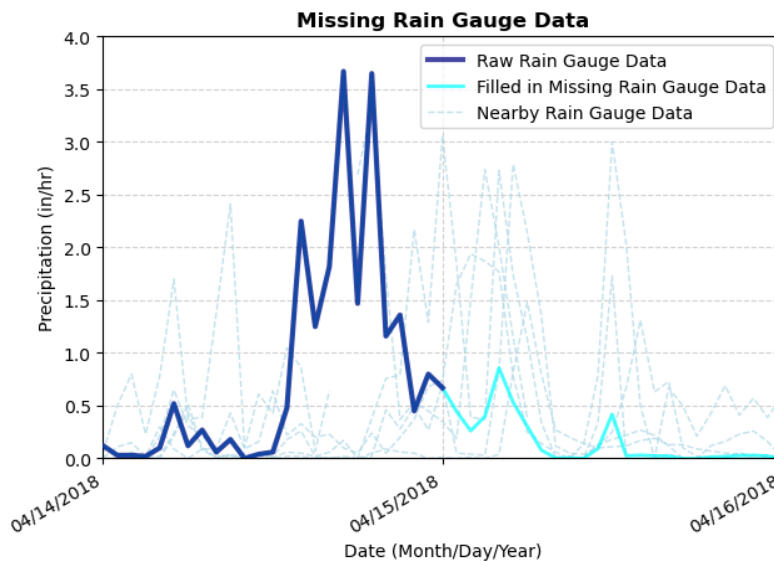


**Figure 4:** The dark blue line represents precipitation captured by the rain gauge, while the light blue line represents the missing rain gauge data that was filled using the normal ratio method. The dashed light blue lines show the rain gauge data used to calculate and fill in the missing rain gauge data.

### *2.1.4 Model Boundaries*

The calibration and validation basin seen in Figure 5 was made with a 40-meter grid size model, while the inset model used a higher resolution grid size for more detailed flood map outputs. The map in Figure 5 shows the boundaries for calibration and validation as well as the gauge locations, and additional information about each gauge can be found in Table 10 of Appendix E. Rain gauge data was used to force streamflow in the calibration and validation simulations. The stream gauge data recorded at the USGS 16103000 stream gauge provided the observations for calibration and validation.

The inset model feature in GSSHA speeds up the computation time and increases the flood map resolution within prioritized areas of flooding. The inset model consisted of a 40-meter grid size model in the upper portion of the watersheds and a 10-meter grid size model along the coast. Figure 5 shows the boundaries of the 10-meter and 40-meter grids in the inset model. The 40-meter grid runs a simulation with the entire area of the 10-meter boundary inside of it. The overland depth and stream flow produced by the 40-meter grid is then computed at the boundary of the 10-meter model. The streamflow and overland depth calculated at the boundary becomes the forcing for the 10-meter grid. The 10-meter grid produces a much higher-resolution flood map output along the coastline, which is necessary for evaluating sea level rise in compound flooding events. The streamflow from the USGS 16103000 stream gauge and the precipitation recorded at the rain gauges around Hanalei Bay were used as drivers of pluvial flooding in the inset model.

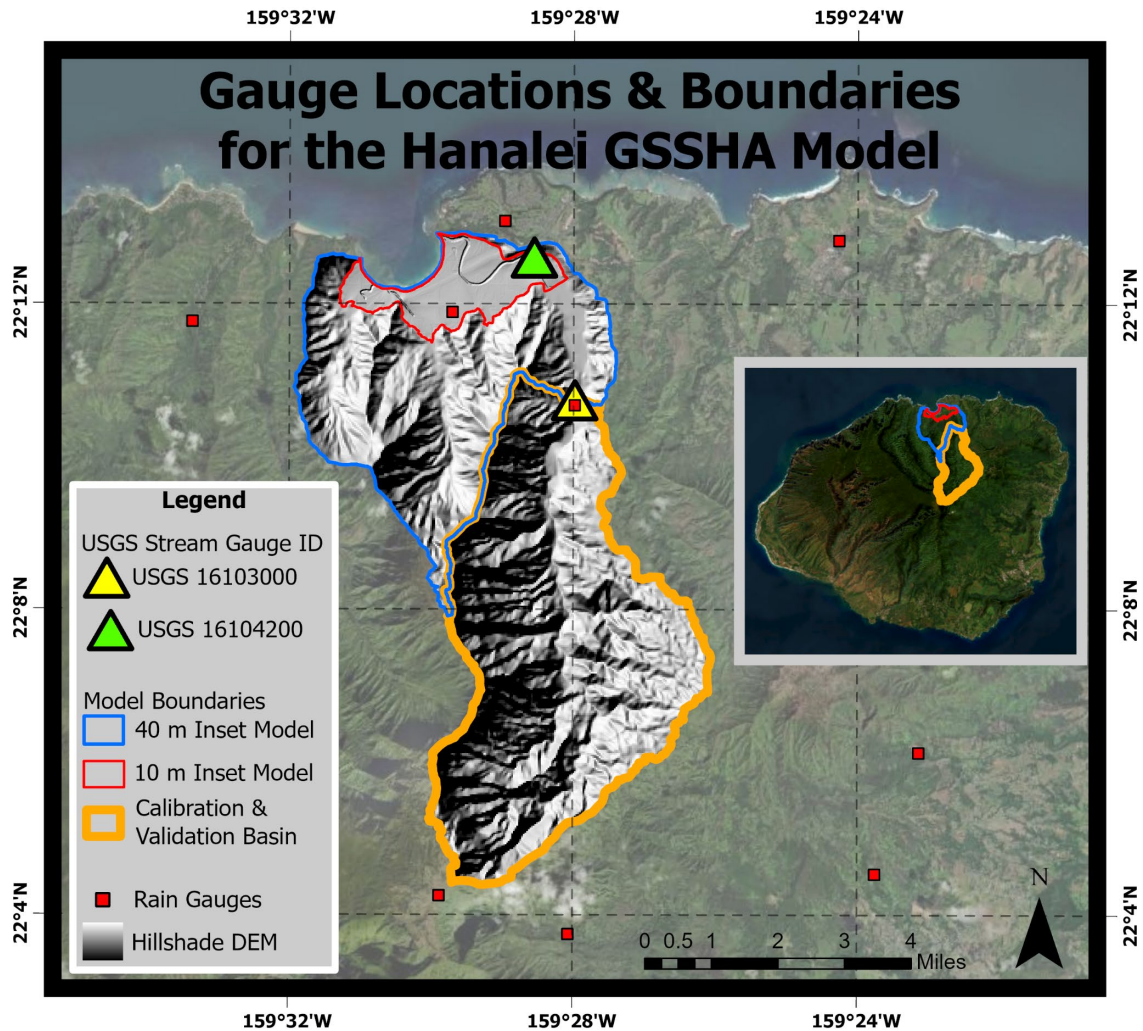


Figure 5: This map shows the model’s boundaries and the stream (2) and rain gauges (9) used for input data. The three model boundaries include the basin for calibration and validation and the two different resolution models grouped into the inset model.

### 2.1.5 Model Setup for Calibration and Validation

The stream gauge (USGS 16103000) in the middle of the Hanalei watershed was used to calibrate and validate the model’s streamflow (Figure 5). As stated in the previous section, the calibration and validation basin was set up with a 40-meter grid size. The stream gauge (USGS 16104200), located closer to the coastline, has gauge height data from 2019 to 2024 but doesn’t include streamflow. For this reason, streamflow measured at the stream gauge (USGS 16103000) was used for calibration and validation. GSSHA outputs the model’s streamflow at a specific drainage outlet. The drainage outlet in the model was set at the same location as the USGS 16103000 stream gauge for calibration and validation. The model’s streamflow output at the

drainage outlet was compared to the observed streamflow at the USGS 16103000 stream gauge for calibration and validation. The model was calibrated and validated using ten extreme precipitation events between 2008 and 2018. The calibration used six events, and the validation used four events, as detailed in Table 2. Various streamflow responses contributed to enhancing the accuracy of the calibration and validation.

**Table 2:** This table contains the ten extreme precipitation events used for calibration and validation. Additional information from the USGS 16130000 is provided for further detail about each event.

Start Date (00:00)	End Date (00:00)	# of Streamflow Peaks	Max Streamflow (ft <sup>3</sup> /sec)	Validation or Calibration	Return Period (USGS Stream Stats Tool, 2024)
12/10/2008	12/15/2008	3	10,900	Validation	< 2 years
12/09/2010	12/11/2010	1	12,700	Validation	< 2 years
09/04/2015	09/06/2015	1	16,700	Validation	2-5 years
12/29/2018	12/30/2018	1	23,600	Validation	5-10 years
07/22/2009	07/25/2009	2	6,403	Calibration	< 2 years
05/08/2011	05/11/2011	3	11,900	Calibration	< 2 years
12/01/2016	12/05/2016	2	18,100	Calibration	2-5 years
11/29/2017	12/01/2017	1	20,100	Calibration	2-5 years
10/31/2017	11/02/2017	2	23,100	Calibration	5-10 years
04/14/2018	04/17/2018	1	31,300	Calibration	10-25 years

## 2.2 Calibration

Before applying scenario simulations, model parameters need to be calibrated so that predictions closely replicate the observed watershed response (Tolson and Shoemaker, 2007). The three main parts of calibration include selecting the appropriate calibration data, selecting the objective function that measures the error between the model predictions and the calibrated data, and selecting the algorithm used to optimize the objective function (Singh and Woolhiser, 2002). Different objective functions produce different calibration results. Servat and Dezetter (1991) determined the Nash-Sutcliffe efficiency to be the best objective function for calibrating a surface water model, whereas Rao and Han (1987) found the least-squares criterion to be the most effective. There are different optimization algorithms as well. The shuffled complex evolution algorithm is recommended by the GSSHA user manual (Downer and Ogden, 2006)

and used in the watershed modeling software made by Aquaveo. The shuffled complex evolution has proven effective and efficient in locating the globally optimum hydrologic model parameters (Sorooshian et al. 1993). Still, the number of simulations for calibration can run into the thousands.

Downer and Ogden (2006) recommended using one long simulation for calibration, but it was more efficient to calibrate the model using extreme streamflow events. The model was calibrated using the six extreme precipitation events shown in Table 2. These events differ in duration, streamflow magnitude, and number of streamflow peaks. The surface roughness, defined by the land use, is one of the most sensitive parameters in GSSHA (Downer and Ogden, 2006). For this reason, the land use that occupies the highest percentage of the model’s area (Evergreen Forest) was calibrated to improve the streamflow response. Literature sources suggested using three different Manning’s n roughness coefficients for the Evergreen Forest land use. Medeiros et al. (2012) suggested using 0.047, USACE (2020) suggested 0.11, and Kalyanapu (2009) suggested 0.32. The three roughness coefficients were simulated in the six extreme precipitation events. The Nash-Sutcliffe Efficiency (NSE) was the objective function used to evaluate the model’s performance (Equation 2). The six events’ NSE values were averaged to estimate the roughness coefficient’s performance. The roughness coefficients with the highest average NSE were selected for use in the final model. The optimal roughness coefficient was then used in the validation simulations.

**Equation 2: Nash Sutcliffe Efficiency (NSE):** This equation was taken from Ahmadisharaf et al. (2019). NSE measures the fraction of the variance of the observed flows explained by the model in terms of the relative magnitude of the residual variance to the variance of the flows. A perfect fit for NSE would be 1.0, and the values should be greater than 0.0.

$$NSE = 1 - \frac{\sum_{i=1}^n (O_i - P_i)^2}{\sum_{i=1}^n (O_i - \bar{O})^2}$$

$O_i$  = Observed Streamflow  
 $P_i$  = Modeled Streamflow  
 $\bar{O}$  = Average Observed Streamflow  
 $\bar{P}$  = Average Modeled Streamflow  
 $n$  = Number of data

## 2.3 Validation

### 2.3.1 Streamflow

Statistics that are widely accepted by hydrologic modelers were used to validate the model’s streamflow. The extreme precipitation events used for validation differ from those used

for calibration (Table 2). The performance was evaluated using varying magnitudes of streamflow events between 2007 and 2020. The variation of events ensures the model performs well under different precipitation and streamflow data (White and Chaubey, 2005). Statistics that are widely accepted by hydrologic modelers were used to compare the observed and modeled streamflow. The model's performance was determined using the following statistical performance measures: Nash-Sutcliffe efficiency (Equation 2, Nash and Sutcliffe 1970), Percent bias (Equation 3), Percent Error (Equation 4), and the Kling-Gupta Efficiency (Equation, Gupta et al., 2009). Other measurements for streamflow validation included the error in peak streamflow (Ahmadisharaf et al., 2019) and the error in the timing of the peak (Titterington et al., 2017). Many other researchers used these statistics to validate GSSHA models (Brendel et al., 2021; Sith and Nadaoka, 2017; Furl et al., 2018; Manrique et al., 2021). The acceptable statistic values for hydrologic models are shown in Table 3. The NSE rating is often used for monthly time steps, so models with shorter time steps are expected to generally have lower performance (Moriassi et al., 2007).

**Equation 3: Percent Bias (PBIAS):** This Equation was taken from Ahmadisharaf et al. (2019). PBIAS measures the tendency of the model output to be smaller or larger than observations. A perfect fit for PBIAS is 0.0, and any value above or below corresponds to overestimation or underestimation, respectively.

$$PBIAS = \frac{\sum_{i=1}^n O_i - P_i}{\sum_{i=1}^n O_i} * 100$$

$O_i$  = Observed Streamflow  
 $P_i$  = Modeled Streamflow  
 $n$  = Number of data

**Equation 4: Percent Error (PE):** The percent error equation analyzes how close a measured value is to the actual value. This equation uses the maximum streamflow output of the model and observations. The sign of the percent error reveals whether the model's peak streamflow was larger than (+) or less than (-) the observed value.

$$Percent\ Error = \frac{P_{max} - O_{max}}{O_{max}} * 100$$

$O_{max}$  = Maximum Observed Streamflow  
 $P_i$  = Modeled Streamflow  
 $\bar{O}_i$  = Average Observed Streamflow

**Equation 5: Kling-Gupta Efficiency (KGE):** This equation was taken from Knoben et al. (2019). It addresses shortcomings in NSE and is used widely in hydrologic modeling for calibration and validation. The values range from negative infinity to 1.0, with 1.0 being a perfect match.

$$KGE = 1 - \sqrt{(r - 1)^2 + \left(\frac{\sigma_p}{\sigma_o} - 1\right)^2 + \left(\frac{\bar{P}}{\bar{O}} - 1\right)^2}$$

$\sigma_o$  = Observed Streamflow Standard Deviation  
 $\bar{O}$  = Average Observed Streamflow  
 $\sigma_p$  = Modeled Streamflow Standard Deviation  
 $\bar{P}$  = Average Modeled Streamflow  
 $r$  = Maximum Modeled Streamflow

**Table 3:** The hydrologic statistics and the acceptable values for the model’s streamflow performance are listed in the table above.

Hydrologic Statistic	Acceptable Value Thresholds	Source
Nash-Sutcliffe Efficiency (NSE)	> 0.5	Moriasi et al. (2007)
Percent Bias (PBIAS)	> 0.0	Moriasi et al. (2007)
Peak Streamflow Percent Error	Within -25% and %25	Ahmadisharaf et al. (2019)
Peak Streamflow Time Error	Within -0.5 to 0.5 hours	Titterton et al. (2017)
Kling-Gupta Efficiency	> 0.0	Knoben et al. (2019)

### 2.2.2 Gauge Height

Gauge height validation assessed the model’s gauge height performance. The gauge height data for the extreme precipitation event of March 2020 was used to predict the USGS 16104200 stream gauge observations (Figure 5). A time series of water depth data from the model’s gridded flood maps was used to compare the modeled and observed gauge height. The modeled gauge height was shifted to match the datum of the USGS gauge. The average gauge height was calculated for both the modeled and observed height. Then, the average difference was used to shift the modeled gauge height to match the datum of the observed gauge height. This height difference was not used to add a correction to the final flood maps, as it was only used to validate the model’s gauge height output. The observed and modeled gauge heights were validated using an NSE value.

### 2.2.3 Satellite Imagery

The model’s flood maps were validated using satellite imagery of specific flood events. Brakenridge and Kettner (2018) used the Sentinel 1 satellite image from 6:30 am on April 15th, 2018, to map the flood inundation in the Hanalei watershed. For reference, this event had a

return period of approximately 25 years (USGS StreamStats, 2024). This precipitation event was simulated in the model to get the modeled flood map from 6:30 am on April 15th, 2018. The model's simulation used an arbitrary threshold value of two inches to define which areas were flooded. The flood inundation area of the satellite imagery was compared to the modeled flood. The three categories of comparison include: the area of flooding observed by the satellite imagery and the model, the area of the modeled flood that isn't shown in the satellite imagery, and the area of flooding shown in the satellite imagery but not in the model.

The F index and C index equations (Equation 6) were used to evaluate the performance of the model's flood extent. Liu et al. (2019) used these equations to assess parameter sensitivity of flood prediction. Both indexes range from 0 to 100 percent. A value of F or C equal to 100 means a perfect match between the observed and predicted flood inundation areas. A lower F score implies a discrepancy between the observed and simulated flood inundation area. The C index describes the percentage of the simulated flood extent correctly predicted by the model output. A low C value means the modeled flood inundation area misses the flood inundation in the satellite imagery.

**Equation 6:** F and C index equations taken from Liu et al. (2019)

$$F = 100 * \left( \frac{A_{om}}{A_o + A_m - A_{om}} \right)$$

A<sub>o</sub> = Observed flooding from satellite imagery  
A<sub>m</sub> = Modeled flooding  
A<sub>om</sub> = Modeled and observed areas of flooding

$$C = 100 * \frac{A_{om}}{A_o}$$

### 2.3 Parameter Sensitivity

Before calibrating the roughness coefficients, the model's performance was evaluated using with different infiltration processes. Three parameterization methods were compared: two models with varying methods of infiltration and a model without infiltration. The Green and Ampt single-layer and multilayer settings in GSSHA are the two infiltration processes used. The sources for the soil texture map and parameter values listed in Table 4 were used to set up two different infiltration processes in the model. The parameter values for the single and multilayer

infiltration processes can be found in Tables 11 and 12 of Appendix F. The single-layer soil texture map from USDA (2019) defined the soil textures for the Green and Ampt single layer infiltration process. Each soil texture from USDA (2019) included the following soil properties for the model: field capacity, wilting point, soil horizon thickness, and hydraulic conductivity. Rawls et al. (1983) provided each soil texture’s porosity and wetting front capillary pressure parameters. Brooks and Corey (1963) had a table that included the soil texture’s pore-size distribution index and residual water content. The soil parameters used for the Hawaiian watershed model by Safeeq and Fares (2012) helped fill in missing soil parameters for the model. Multilayer infiltration used the same parameters as the single layer infiltration process but each soil layer’s hydraulic conductivity and thickness was varied. The USDA (2019) engineering properties table has data for each soil layer’s thickness and hydraulic conductivity. All other parameters that were used in single layer infiltration was held constant for each soil’s layers: field capacity, wilting point, porosity, wetting front capillary pressure, pore size distribution index, and residual water content.

**Table 4:** The sources of the soil texture map and the parameter values are listed in this table.

<b>Infiltration Parameters</b>	<b>Data</b>	<b>Resolution</b>	<b>Source</b>
Soil Texture Map	USDA SSURGO Soil Properties	10 m	USDA (2019)
Soil parameters: field capacity, wilting point, soil horizon thickness, texture, and hydraulic conductivity	USDA SSURGO Soil Properties tables		USDA (2019)
Soil parameters: porosity and wetting front capillary pressure	Table relating soil texture to porosity and wetting front capillary pressure		Rawls et al. (1983)
Soil parameters: pore-size distribution index and residual water content	Table relating soil texture to pore-size distribution index and residual water content		Brooks and Corey (1963)
Missing soil parameters	Input soil data for a Hawaiian watershed model		Safeeq and Fares (2012)

Infiltration processes for the model had the highest sensitivity to the model’s streamflow response. The infiltration processes caused the model to produce lower streamflow outputs compared to the observations. The multi-layer infiltration processes had the closest match to the

observed streamflow but still had consistently lower streamflow peaks compared to a ‘concrete’ model that did not have infiltration (Figure 6). Also, the soil parameters were not validated in the field, so there was some uncertainty. Infiltration processes were not necessary for achieving an acceptable streamflow output.

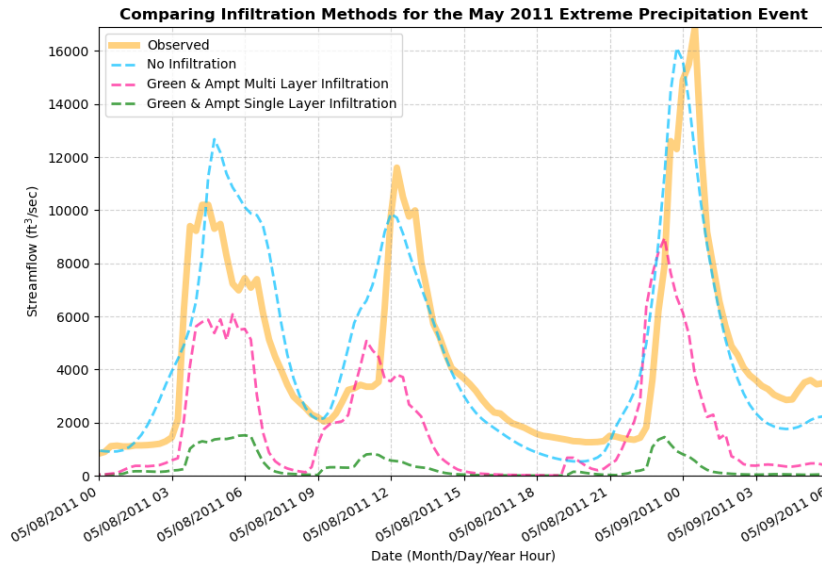


**Figure 6:** This graph evaluates the model’s streamflow performance using different infiltration methods.

## 2.4 Compound Flooding Scenarios

### 2.4.1 Extreme Precipitation

Four extreme precipitation events that occurred between the years of 2017 and 2020 were used in the compound flooding scenarios. These events are not the same as the calibration or validation simulations. The water height data from the USGS 16103000 stream gauge was used to determine four extreme precipitation events. These events provided precipitation scenarios for compound flood modeling. Local community organizations in Hanalei and the NOAA National Weather Service indicated that the Hanalei Bridge closes when the USGS stream gauge 16103000 reaches 5.5 - 7.0 feet due to the river overtopping the banks and flooding the roadway on the west side of the bridge. The events ranged from the minimum height of the Hanalei Bridge closures (6 feet) and the maximum height recorded (18 feet) with an interval of four feet (6 ft., 10ft., 14ft., and 18 ft.). According to NCEI, each gauge height event in Table 5 was also

recognized as a flooding event in Hanalei (Table 13 of Appendix G). Other information, including the return period, maximum streamflow, and actual peak height, is provided in Table 5. The graph in Figure 7 shows the similar hydrograph shapes of the four gauge height events.

**Table 5:** This table lists the gauge height peaks and the event date. The gauge height scenario is the height referred to in this report. A complete list of all return periods given by the USGS StreamStats Tool for station number 16103000 is shown in Table 14 of Appendix H.

Gauge Height Event (ft)	Actual Peak Height (ft)	Date of Peak	Maximum Streamflow (ft <sup>3</sup> /sec)	Return Period (USGS StreamStats Tool, 2024)
6	6.02	11/17/2018	3,800	< 2 year
10	10.01	11/17/2019	11,700	< 2 year
14	13.66	11/30/2017	20,100	2-5 years
18	17.65	03/28/2020	30,500	10-25 years

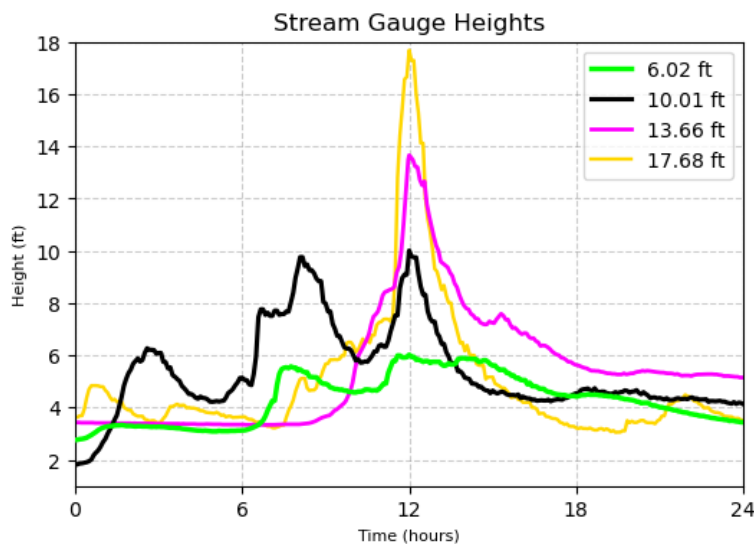


**Figure 7:** This figure shows the hydrographs of the four gauge height events used for the compound flooding scenarios.

The rain gauges and streamflow data from the USGS 16103000 stream gauge was used to force runoff in the model. By using streamflow at this gauge, the model area and computation time of the inset model was decreased. Also, the accuracy of the precipitation interpolation increased due to the denser network of rain gauges in the lower portions of the watersheds (Figure 5). Rain gauges were used to force runoff along the coastline and the other watersheds that drain into Hanalei Bay. The sea level height along the coastline boundary was the only variable that changed during each of the four gauge height simulations.

### 2.4.2 Sea Level

Three sea level scenarios were combined with the four gauge height events (Table 5) to simulate twelve compound flooding scenarios. The three sea level scenarios and the methodology for determining them are shown in Table 6. The model boundary along the coastline was set up as a general head boundary, and the constant stage height was changed for each sea level scenarios. The model was spun up for 24 hours to allow the sea level to reach equilibrium before the precipitation runoff interacted with the boundary. NOAA’s Sea Level Projection tool (NOAA Sea Level Projection, 2024) used the water level data from the Nawiliwili 1611400 buoy to predict sea level rise. It is important to note that sea level rise predictions for Hanalei are from the Nawiliwili 1611400 buoy, located on Kaua’i’s southeast side. Because the exact date of the DEM survey is unavailable, the publication year of the DEM (2013) is the datum for the mean sea level. The height the sea level has risen between the year of NOAA’s prediction and the publication of the DEM was not included. Also, the sea level rise scenarios do not include the mean higher high water. The maximum water level recorded at the Nawiliwili 1611400 buoy was used for the extreme sea level scenario (Figure 8). The maximum water level represents storm surge height during the landfall of Hurricane Iniki (09/11/1992).

**Table 6:** This table describes the three sea level scenarios (0 ft, 4.0ft, 8.2ft) and how the sea level heights were chosen.

Sea Level Scenario (ft)	General Description	Derivation of Sea Level Scenario
0	Mean sea level at the time of the DEM publication	Baseline sea level scenario representing present-day conditions.
4.0	Sea level rise in 2100	The sea level rise was based on the upper limit of the likely range (83rd percentile) for the year 2100 based on IPCC AR5 RCP8.5 projections.
8.2	Sea level rise in 2100 and historical storm surge	The maximum storm surge height above mean sea level was 4.2 feet during Hurricane Iniki's landfall in 1992. The storm surge (4.2 ft) and the expected sea level rise (4.0 ft) resulted in an 8.2 ft sea level height.

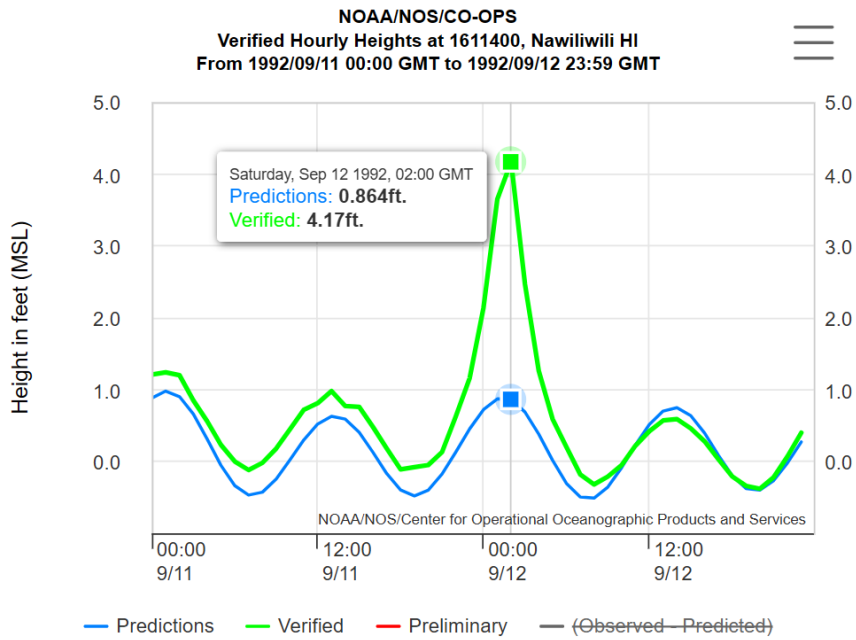


**Figure 8:** This screenshot shows water level height data from the Nawiliwili 1611400 buoy when Hurricane Iniki passed over Kaua‘i. The maximum storm surge height reached nearly 4.2 feet.

## 3.0 RESULTS

### 3.1 Calibration

As stated in section 2.3.1, the model was calibrated with six streamflow events using the suggested Evergreen Forest rough values (0.047, 0.11, 0.32) . The average NSE value from the six extreme precipitation events is shown in Table 7. The graph in Figure 9 shows all NSE values for the calibration simulations, and the exact values can be found in Table 15 of Appendix I. The roughness value that Medeiros (2012) suggested for the Evergreen Forest land use produced the highest average NSE value (0.633) in the model. USACE (2020) recommended using 0.11 for Evergreen Forest land use in Hawai‘i based on visual observations of an O‘ahu watershed. The lowest roughness value (0.047) suggested by Medeiros (2012) enhances the model’s performance. Figure 16 of Appendix J shows the graphs of each calibration simulation using the 0.047 roughness value for the ‘Evergreen Forest’ land use. A roughness value of 0.047 for the ‘Evergreen Forest’ land use was used as the final parameter in the model.

**Table 7:** This table shows the three different roughness coefficients and the average NSE value associated with each set of extreme precipitation simulations.

<b>Evergreen Forest Manning’s n Roughness</b>	<b>Average NSE from Calibration</b>
0.047 (Medeiros, 2012)	0.633
0.11 (USACE, 2020)	0.575
0.32 (Kalyanapu, 2009)	0.275

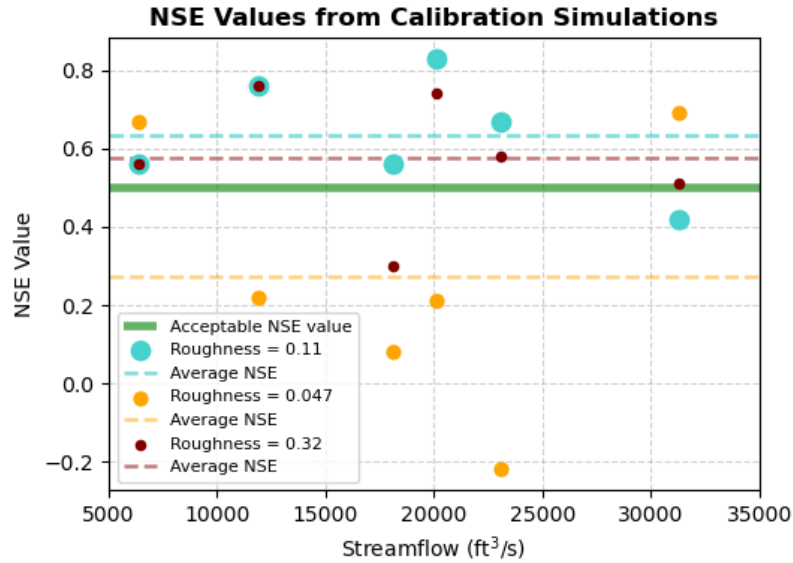


**Figure 9:** This graph displays the NSE value for the six calibration simulations. The thick green line represents the threshold for acceptable NSE values ( $> 0.5$ ). The groups of six colored points represent simulations run with the same roughness value. The colored dashed lines show the average NSE values for each group of roughness simulations.

## 3.2 Validation

### 3.2.1 Streamflow

The model was validated with the streamflow at the USGS 16103000 stream gauge (Figure 5), using four extreme precipitation events between 2008 and 2018 (Table 2). The performance statistics for each validation simulation is displayed in Table 8, and a graph showing the modeled and observed streamflow from one event can be found in Figure 10. All of the graphs for the validation simulations can be found in Figure 16 of Appendix J. Table 8 shows the validation simulations had high NSE values and most other statistics values were acceptable based on the literature (Table 3). The two events between 2008 and 2010 had a higher NSE value than the others, possibly due to a more accurate precipitation interpolation.

**Table 8:** The streamflow validation simulations’ performance statistics can be found in this table. The statistics include Nash Sutcliffe Efficiency (NSE), Kling-Gupta Efficiency (KGE), Percent Bias (PBIAS), peak streamflow percent error, and maximum streamflow time error. The shaded green values represent the acceptable performance values according to the literature described in **Table 5**.

Validation Simulation Start Date	Observed Peak Streamflow (ft <sup>3</sup> /sec)	NSE	KGE	PBIAS (%)	Peak Streamflow % Error	Max Streamflow Time Error (hr)
12/13/2008	10,900	0.86	-0.19	-15.67	10.27	0.25
12/09/2010	12,700	0.85	-0.15	-13.32	-19.84	0.45
09/04/2015	16,700	0.53	0.16	21.38	-47.75	-0.58
12/29/2018	23,600	0.71	0.26	32.53	-53.23	0.42

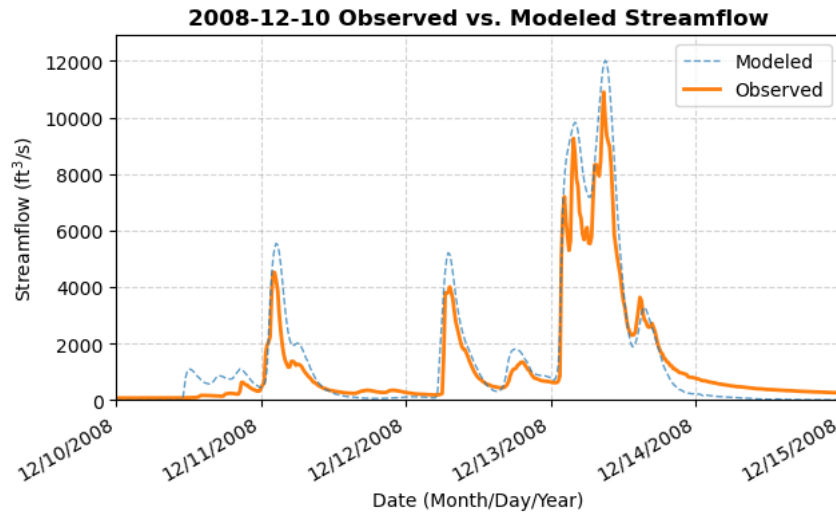


**Figure 10:** This graph shows the December 2008 validation event. The modeled (dashed blue) and observed (solid orange) streamflow at the USGS 16103000 station are plotted in this graph.

### 3.2.2 Gauge Height

Figure 11 shows the observed and modeled gauge height from the extreme precipitation event of March 2020. A slight correction to the model’s gauge height (+3.53 feet) was needed to fit the observed gauge height’s datum. It appears the model simulates a gauge height similar to what is observed (Figure 11). The first twelve hours data in Figure 11 was omitted from the NSE calculation to allow the model to warm up. The NSE value for this simulation was 0.62 According to Moriasi et al. (2007), this value is above the acceptable value for hydrologic

modeling. Only one simulation was tested, so it is unsure how the model's gauge height performance would compare for other events.

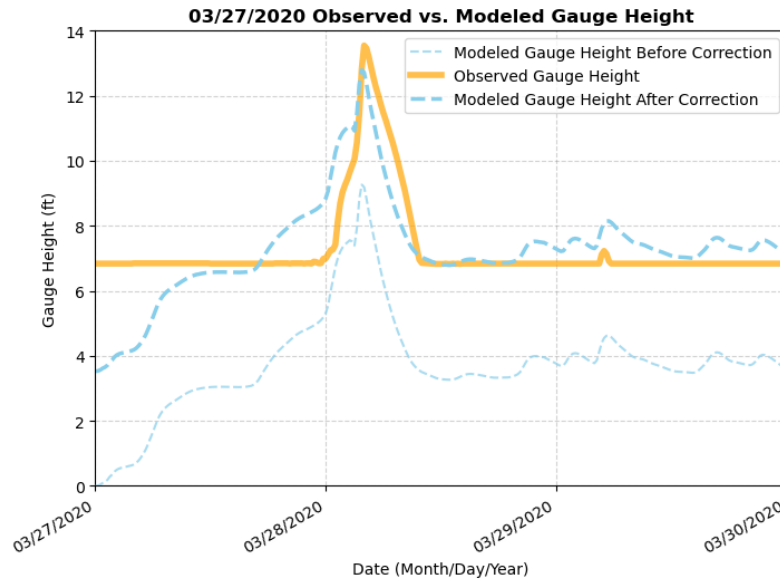


**Figure 11:** This graph shows the modeled and observed gauge height used for validation. The modeled gauge height data was corrected to match the datum of the observed gauge height recorded at the USGS 16104200 stream gauge.

### 3.2.3 Satellite Imagery

The comparison map shown in Figure 12 displays where the modeled flood extent overestimates, underestimates, or perfectly fits the satellite observed flood extent (Brakenridge and Kettner, 2018). The C and F index for the modeled and observed flood maps was 53.2% and 29.3%, respectively (Equation 6). The low C and F index indicates discrepancies between the modeled and observed flood areas. As seen in Figure 12, the model underestimates the amount of flooding in Hanalei Valley and overestimates flooding in the center of the town near the coast. The model's fit to the observed flood area improves when the maximum flood grid of the entire simulation is used. The maximum flood grid is not an appropriate representation of what occurred at the time the Sentinel 1 satellite image was taken, but it shows the flood inundation area does increase to the extent of the satellite imagery. The C index for the maximum flood grid map is just under 94%. At some point in the simulation, the flood extent covers most of the areas shown in the satellite imagery.

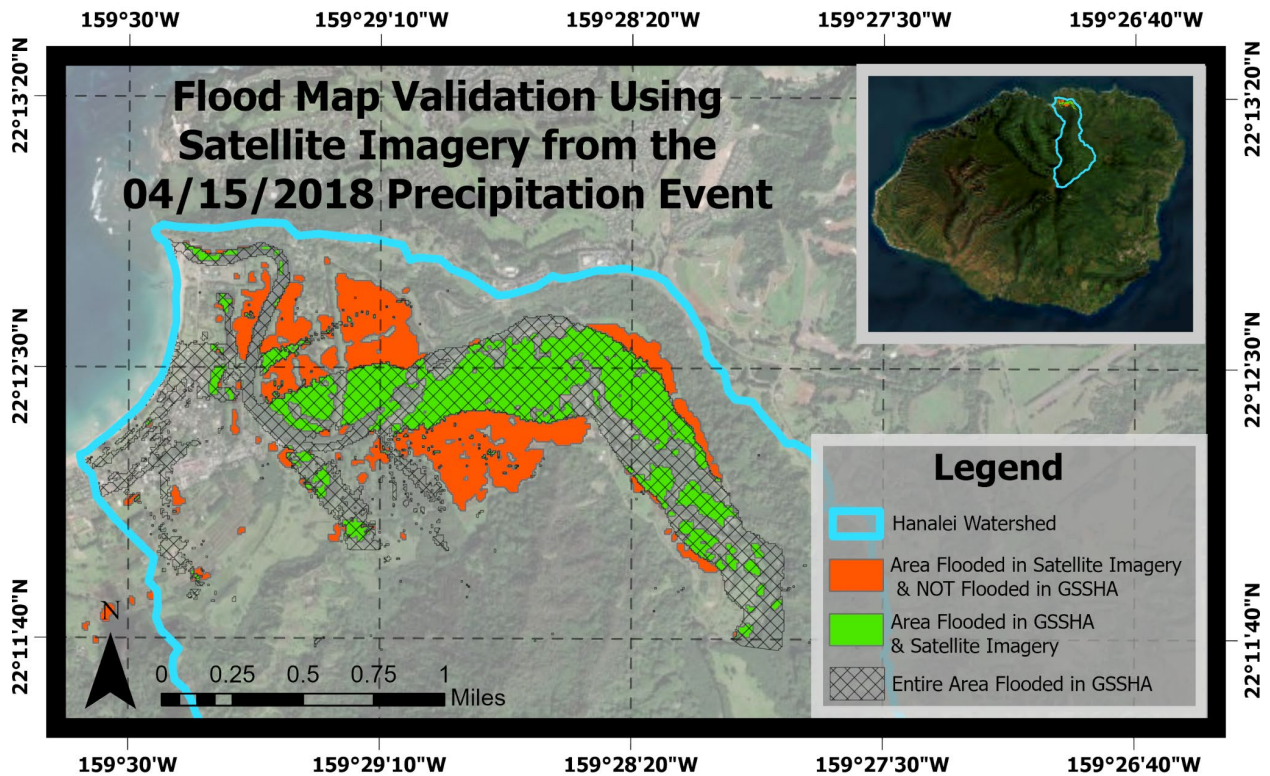


**Figure 12:** This map compares the modeled and satellite-observed flood inundation area created by Brakenridge and Kettner (2018). The green area shows where the GSSHA’s flood map fits the satellite imagery flood area. The orange/red area represents the area observed to be flooded in satellite imagery but not in GSSHA. The hatched area beyond the green area represents the area flooded in GSSHA but not in the satellite imagery.

### 3.3 Compound Flood Maps

The compound flooding scenarios (Table 5 and 6) highlight the areas that are most exposed to backwater effects. Parcel data from the Hawai‘i Statewide GIS Program (2024) was used to evaluate the changes in flood extent. Half a foot of water was used as a threshold to define flooded areas and calculate the total number of parcels flooded. The model shows that the total number of flooded parcels increases when compound flooding occurs. The higher sea level will cause more water to back up and spill out of the river channels near the coast. Figure 13 highlights how the 6-foot gauge height and an 8.2-foot sea level scenario (storm surge and sea level rise) could flood nearly the same number of parcels as the 10-foot gauge height at the

current mean sea level (0 feet). This output from GSSHA hints that the lesser extreme precipitation events may be a more outstanding issue in the future.

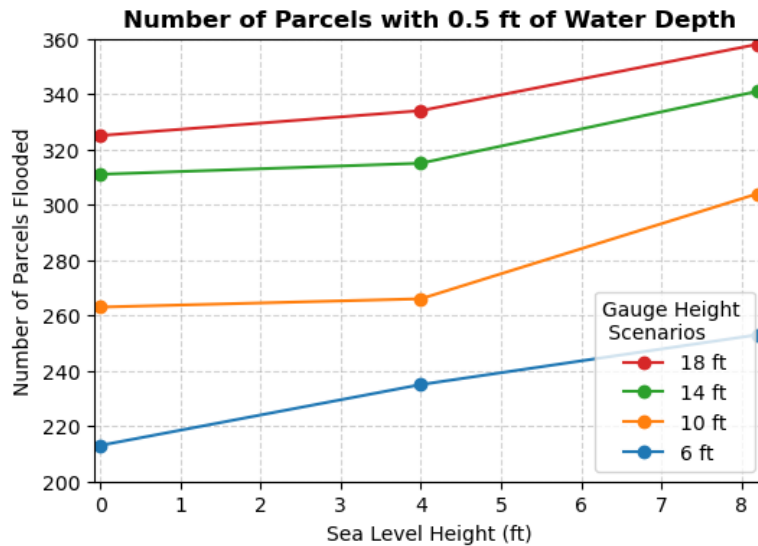


**Figure 13:** Each point represents the total number of parcels (Hawai'i Statewide GIS Program, 2024) flooded with half a foot of water. Each colored line represents the various gauge height events used in the compound flooding.

The model showed that a higher sea level will increase flooding along the coastline, coastal river channels, and areas around the Hanalei River. The maps in Figure 14 highlight the three areas of increased flood inundation. All gridded flood depth maps for the compound flood scenarios can be found in Figure 17 of Appendix K. The red and blue polygons in Figure 14 represent the flooding area that does not receive a massive influence from precipitation, whereas the yellow polygons represent the area of flooding that grows in size from the intensity of the precipitation. Increases in water depths along the coastline and the lower reaches of the river channels were primarily from the higher sea level rather than the compounding effects of extreme precipitation. The simulations showed that the floodplains adjacent to the Hanalei River are most exposed to compound flooding effect. The yellow polygons in Figure 14 show that as the severity of the precipitation event increases, the backwater effects from the combination of sea level rise become more significant.

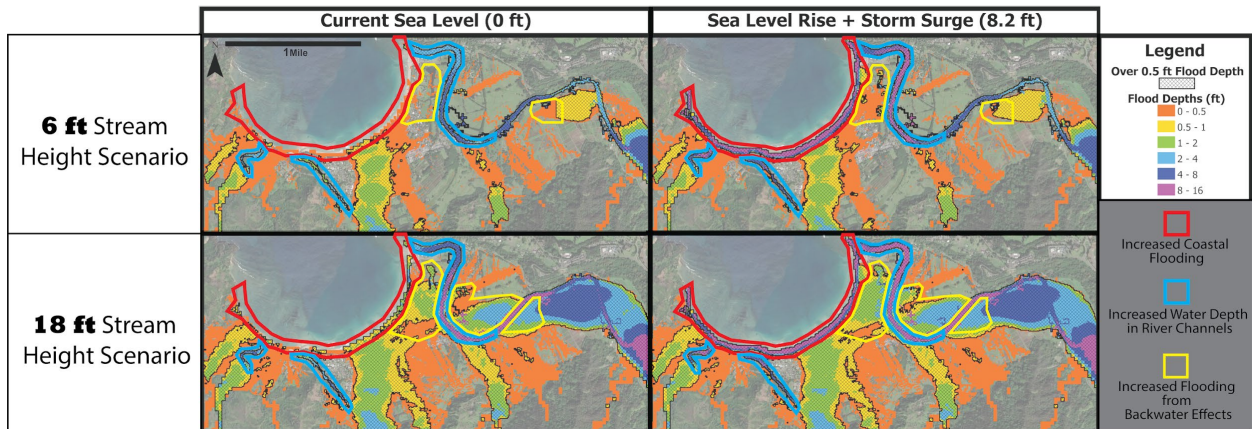


**Figure 14:** The red, blue, and yellow outlined polygon areas represent the extent of additional flooding when a higher sea level is simulated in the model. The area of the hand-drawn polygons were determined based on the changes in flood depths between sea level rise simulations.

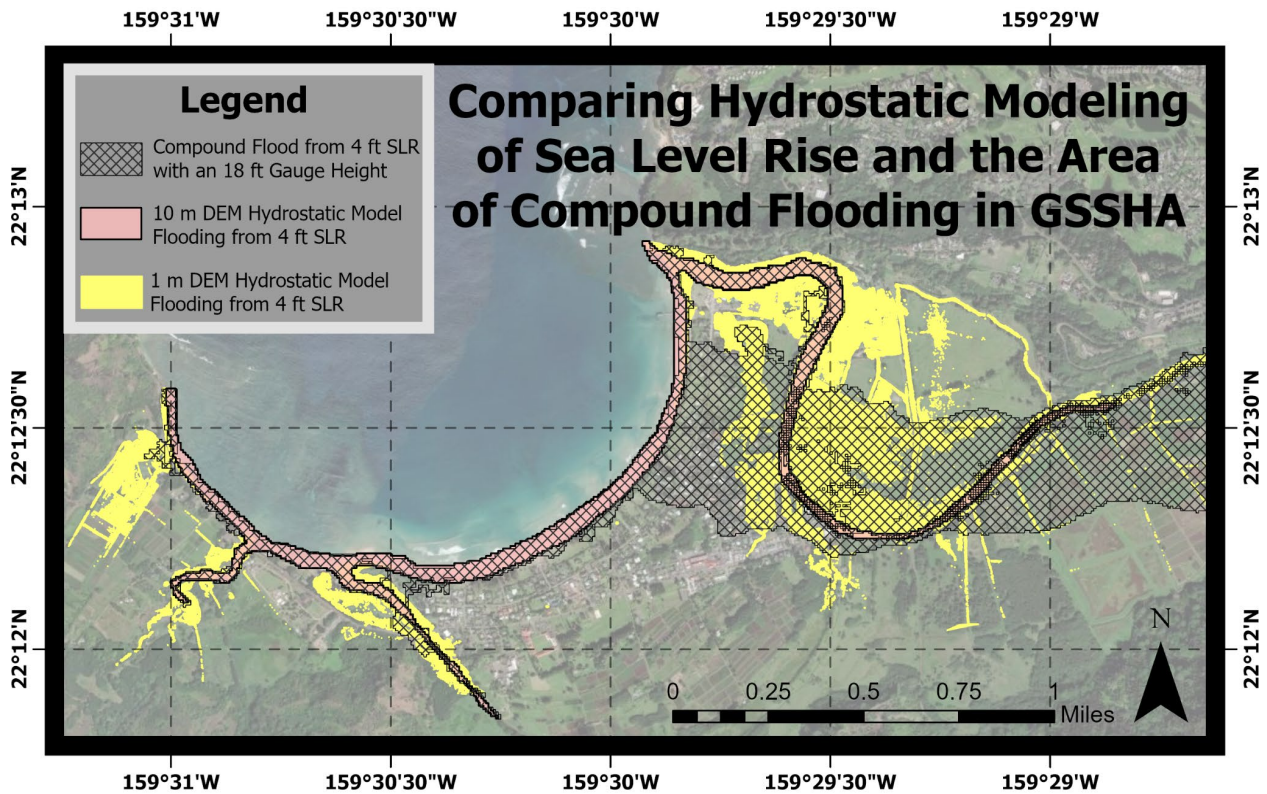


**Figure 15:** This map shows the extent of flooding from a 4-foot sea level rise in a 10-meter resolution (USGS, 2013) and 1-meter resolution (Hawai‘i Statewide GIS Program, 2021) hydrostatic model. The hatched area represents the extent of additional flooding from sea level rise from an 18-foot gauge height GSSHA simulation.

Compound flood models can identify where sea level rise causes an increase in extreme precipitation flooding. The area of increased flood depths is greater than the area of just sea level rise alone (Figure 15). The extreme precipitation runoff builds up the water level of the receiving water body (ocean). When sea level rise generates an upstream-propagated energy head, the two interact to back up the flow of water, causing more flooding. The hatched layer in Figure 15 shows the extent of increased flooding caused by the interaction of sea level rise and extreme precipitation. The hatched layer represents the area of increased flooding when an 18-foot gauge height event is simulated with sea level rise (4 ft.).

The size of this hatched layer depends on the intensity of the extreme precipitation event and is also a direct influence of the DEM resolution in the model. The pinkish-orange area in Figure 15 shows the passive flooding from a 4-foot sea level rise in a hydrostatic model using a 10-meter DEM (USGS, 2013). Sea level rise causes a significant increase in flooding around the Hanalei River when extreme precipitation is simulated in the model. On the other hand, areas on the western side of Hanalei Bay exhibit a similar amount of flooding between the hydrostatic model and the compound flood scenario (hatched layer in Figure 15). Hydrostatic models made from different DEM sources and resolutions (1-meter and 10-meter) show differences in flood extents. The passive flooding from sea level rise in the 1-meter hydrostatic model was much more significant than the 10-meter model. Both hydrostatic models showed similar patterns of flooding (Figure 15), but the 10-meter DEM had a smaller flood extent than the 1-meter DEM. Because the GSSHA model uses this 10-meter DEM in its input data, it will underestimate the extent of passive flooding from sea level rise and ultimately underestimate the extent of compound flooding.

## 4.0 DISCUSSION AND CONCLUSIONS

### 4.1 Uncertainties and Limitations

#### *4.1.1 Enhancing Calibration Methods for Improved Flood Predictions*

The model boundary for calibration (Figure 5) may hinder the model's flood predictions in the lower reaches of Hanalei. The upper and lower portions of the watersheds have different land uses (Figure 3). Calibrating the roughness coefficients in the upper Hanalei watershed may cause the model to have lower downstream performance. Hall et al. (2005) performed a detailed sensitivity analysis of different sub-reaches of a river channel, finding that the Manning's  $n$  roughness coefficients has a high spatial influence on model predictions. Using just the 'Evergreen Forest' land use for calibration may not be appropriate for model predictions in the lower watersheds. Calibrating with multiple roughness coefficients would improve the validation performance. Further sensitivity analysis of the roughness coefficients could inform which parameters are most necessary for further calibration (Downer and Ogden, 2006). Gauge height or flood imagery may be a more effective method for calibration.

Calibrating with flooding imagery may enhance the flood-predicting performance of the model because the model boundary for calibration would include all parameters in the lower watersheds. Satellite imagery may be a valuable tool for calibration, but more than just one image of flooding is needed. Liu (2019) provides an example of using Landsat imagery to compare different models' performance at predicting the observed flood, highlighting how changes in the roughness coefficients cause significant differences in the flood extent. Images other than satellite imagery, such as the one shown in Figure 1, could provide an additional observation for calibration or validation. Garrote et al. (2018) showed that imagery of tree scars from a flash flood event can improve the predictions of hydraulic models in ungauged basins. Images of multiple floods are necessary for calibration, as Downer and Ogden (2006) recommend using long simulations with multiple precipitation events to get the full details of the model's performance. Many watersheds in Hawai'i lack stream gauge measurements, so adverse imagery methods may be needed to calibrate new GSSHA models.

Gauge height observations may be more suitable for calibration as they are more closely related to the model's flood map. The gauge height observations from the USGS 16104200

stream gauge could be used for further calibration. Calibration of the basin above the USGS 16104200 stream gauge would include additional land uses and roughness coefficients that influence flooding in the lower portion of the Hanalei watershed. The USGS 16104200 stream gauge also has a long enough data history to include multiple extreme precipitation events for calibration. Six extreme precipitation events were used to calibrate the model, but more than six may be needed to improve the model's validation performance.

#### *4.1.2 Enhancing the Gauge Height Validation*

The datum correction for the gauge height validation (Figure 11) could be enhanced through field observations and accounting for the uncertainty of the DEM. The USGS 16104200 stream gauge's datum causes the model's gauge height to differ by a constant height. The uncertainty measurement for the DEM could cause this shift in the datum. A USGS 16104200 stream gauge survey could give a more accurate representation of this correction. One downside of the USGS 16104200 gauge is that it is in a highly dynamic river segment, where the channel geometry changes after extreme flood events. The change in the channel shape may cause the datum to shift after extreme flood events, which may contribute to heterogeneity in the datum correction.

The model's performance was higher for streamflow than gauge height. The average NSE value for the streamflow performance (Table 8) was 0.74, while the only gauge height simulation (Figure 11) produced an NSE value of 0.62. The model's gauge height output had a lower performance, likely from using streamflow for calibration. The USGS 16104200 stream gauge used for gauge height validation is further downstream from the stream gauge (USGS 1610300) used for calibration and has different land uses. Also, the gauge height validation only had one event. Multiple extreme precipitation events should be tested for a more detailed picture of the model's gauge height performance. For example, Brendel et al. (2021) used ten extreme precipitation events to validate a GSSHA model's gauge height and streamflow performance. More events must be tested before this model is acceptable for public use and planning purposes.

#### *4.1.3 Rain Gauge Interpolation and its Effect on Streamflow Validation*

The precipitation interpolation in the model contributes to lower streamflow performance values. A dense spatial distribution of rain gauges is needed for the model to accurately

interpolate precipitation for each simulation due to the spatial variability of precipitation in Hanalei. The GSSHA user manual also highlights that a rain gauge network with inter gauge distances greater than 1.5 miles will not capture the true spatial variability of precipitation (Downer and Ogden, 2006). An inaccurate precipitation interpolation could have affected the model's calibration and streamflow validation results. The model's streamflow performance was correlated with the density of the rain gauge network within the simulation.

A rain gauge located at the USGS 16010300 stream gauge (Figure 6) was a key point of interpolation for the model. It only had a range of data from 2008 to 2011. Recent surface water models for the Hanalei watershed also used this rain gauge for validation. For example, Fortini et al. (2020) used the rain gauge data between October 2007 and October 2011 to validate a Soil and Water Assessment Tool model of Hanalei. Simulations with data from this rain gauge had a much higher performance. If a rain gauge is reinstalled in the middle of the Hanalei watershed, the model would more accurately interpolate precipitation. Installing a new rain gauge may not be practical, but is not a scalable method as a large number of new rain gauges is necessary to scale GSSHA across Kaua'i. A more accurate precipitation interpolation method may be needed (Downer and Ogden, 2006). The radar data from Huang et al. (2022) is somewhat unreliable for Hanalei. Still, it may be an effective precipitation interpolation method for other sides of the island as fewer mountains block the signal. Still, other methods may need to be explored.

Calibrating the model with gauge height observations could eliminate the model's reliance on precipitation interpolation. The USGS 16103000 stream gauge in the upper reaches of the Hanalei River could be used as the discharge forcing in the model. The lower stream gauge (USGS 16104200) could be used for gauge height calibration. The final model would then use streamflow from the USGS 16103000 stream gauge streamflow as a forcing for compound flooding scenarios. This unique calibration method may not be scalable to other watersheds, as it is uncommon for a watershed in Hawai'i to have multiple stream gauges.

#### *4.1.4 Discrepancies Between the Satellite Imagery and Modeled Flood Maps*

The observed streamflow and flood map could differ from an idealized model due to unpredictable factors and hazards during extreme floods, such as landslides and debris dams. When meeting with a member of the Hanalei community, they stated that the speed of the flood wave and the large landslides caused an unusual flood during the April 2018 event. Debris dam

failures and landslides may have occurred in the upper portions of the Hanalei watershed, leading to a higher flow rate than what the idealized model would predict. Ogden (2016) provides an example of using GSSHA to detect landslide-affected peak flows. It is possible the satellite imagery validation is affected by landslides or another phenomenon that GSSHA can't simulate. The model had a lower streamflow performance for this particular event. Table 15 of Appendix I shows the event of April 2018 has lower NSE values for the modeled streamflow. The poor streamflow performance is further evidence that landslides or debris dam failures may have caused discrepancies in the satellite imagery validation.

The resolution of the model decreases the extent of inundation in the model. The 10-meter resolution of the model only captures some of the small ditches and berms that route water to different flood plains outside of the Hanalei River because of the low gradient of the coastal flood plains in Hanalei Bay. There may be greater flood depths and a lesser extent of inundation because there is no ditch or drainage area for the flood waters to transfer. The model's resolution could result in an underestimated flood area. A higher resolution DEM and surface water model could help define some of the essential hydrological features contributing to flooding in Hanalei.

Although the observed flood map derived from the Sentinel 1 satellite imagery looks acceptable, it likely has some errors. The satellite imagery flood map shows no flooding in the Hanalei River. It is possible that Brakenridge and Kettner (2018) removed this inundation area from the flood map, or their methodology didn't capture the flow of water in the river channel. The tall grasses in this region may also limit the extent of flooding that could be viewed by satellite imagery. The tall grass and elimination of flood waters in the Hanalei River channel would cause the satellite image to underestimate the observed flooding area. The C and F index (Equation 6) would report lower percentages, making it appear that the model overpredicts flooding for specific regions.

## 4.2 Effects of DEM Resolution on Sea Level Rise Inundation in the GSSHA Model

The model's DEM resolution is a crucial factor in accurately assessing the inundation from sea level rise. Hydrostatic models in Hawai'i and around the world leverage higher resolution DEMs to achieve the most precise representation of flooding from sea level rise. A higher resolution DEM provides detailed information on the ditches and pathways for flood

inundation. Fereshtehpour and Karamouz (2018) discovered that coarser resolution DEMs or resampling of a higher resolution DEM leads to an overall rise in land elevation, resulting in a smaller inundation area. As depicted in Figure 15, the inundation area is more extensive for hydrostatic models that use a higher-resolution DEM. In low-lying deltaic areas like Hanalei, where the land elevation variation is usually in the order of only a few decimeters, even a slight offset in the elevation data can significantly impact the accuracy of the flood assessment (Van de Sande et al., 2012). The model's operation at grid sizes lower than 10 meters is not feasible, and Hanalei Bay's higher resolution DEM (1-meter) only covers a portion of the modeling area. The GSSHA model's sea level rise prediction underestimates the flood extent compared to higher resolution hydrostatic models.

It is imperative that compound flood models operate at a similar resolution as hydrostatic models to ensure the most accurate assessment of sea level rise inundation. Unlike hydrostatic models, GSSHA or other compound flood models use a lower-resolution DEM or resampling methods because a larger grid size is needed for efficient simulations. The resolution of compound flood models is limited by computation and model capabilities. The computation time of compound flood models also limits their ability to incorporate parameter uncertainty in simulations. Paoa (2023) presents a recent case of integrating DEM uncertainty in hydrostatic modeling on O'ahu. The computation time of compound flood models restricts their ability to incorporate DEM and parameter uncertainty in different simulations. Compound flood models should have similar grid sizes as the hydrostatic models of the study area. Until hydrologic models operate at the same resolution as hydrostatic models, compound flood models will continue to underestimate the extent of flooding from sea level rise, leading to more uncertainty in the gridded flood maps. Understanding the interaction of sea level rise and extreme precipitation flooding is best achieved with the highest resolution models.

### 4.3 Improved Risk Assessment and Mitigation Through Compound Flood Models

County and Statewide planners face the challenge of scaling compound flood modeling to all exposed coastal regions. Compound flood models are data intensive and require long computation times, so creating and updating them takes extra work. Exploring different compound flood models and methodologies is necessary before making island-wide models to ensure that the model outputs suit the hydrologic processes in each watershed. We also recognize

that some regions are more exposed to extreme precipitation than sea level rise and vice versa. Watersheds are highly exposed to multiple flood drivers should be a focus for compound flood modeling. As shown in Figure 14, compound flooding only affected the floodplains of the Hanalei River. Still, it is possible that using a higher resolution DEM would change the model's results. Generally, watersheds with low lying deltaic plains and high discharge peaks are significantly more affected by compound events (Feng et al, 2023). The variation in topography and extreme precipitation floods along the coasts of Hawai'i means compound flood models are only necessary for watersheds with high exposure to multiple flood drivers. Further research should determine which coastal areas or watersheds should be targeted for compound flood modeling.

The flood map results from the model highlight the planning and mitigation uses of compound flood modeling. The increase in sea level will directly affect coastal infrastructure but it will also increase flood inundation extent from extreme precipitation events from enhanced backwater effects (Feng et al., 2022). The lower return period precipitation events will likely continue with sea level rise at the end of the century, so their effect with sea level rise should be considered. Flood maps from compound flood models play a crucial role in identifying areas most exposed to an increase in inundation from compound events. By identifying the additional flooding from backwater effects (Figure 14), the model provides an example of how compound flood simulations can help planners and project managers plan for and mitigate the impacts of sea level rise (Xu et al., 2023). Mitigation projects should consider how sea level rise will affect the longevity of flood mitigation projects. The availability of input data allows GSSHA to be scaled to other coastal regions in Hawai'i. The methodology and results of this study could be scaled to other watersheds in Kaua'i for further research or planning.

#### 4.4 Future Directions for Enhancing Compound Flood Modeling in Hanalei

The DEM uncertainty and vertical resolution in the model needs to be considered for the final gridded flood maps. A different DEM should be used in the model because this information was unavailable for the 10-meter DEM USGS (2013). The higher resolution DEM acquired for a recent Hanalei flood study (HWH and SRGI, 2023) would significantly enhance the accuracy of the model's topography. This river channel geometry in the new high-resolution DEM is more accurate compared to the 10-meter DEM. The benefits of using a higher resolution DEM are

substantial, as it could solve the DEM errors causing the model to flood from the Wai‘oli Stream into the center of Hanalei. The leaders at the NOAA National Weather Service for Hawai‘i and other sources have explained that the flood extent caused by the Wai‘oli Stream in the model is inaccurate. Almost all of the flooding in Hanalei comes from the Hanalei River, not the Wai‘oli Stream. A new DEM may help alleviate this issue. Implementing a new DEM in the model may require further calibration.

The model should be calibrated and validated with gauge height observations or flood imagery. Streamflow does not accurately represent the model's performance because the final output contains water level heights in a gridded flood map. When the model is updated, multiple extreme precipitation events should be used for calibrating and validating with gauge height or imagery. A new sensitivity analysis should be completed for a more thorough calibration. The sensitivity analysis should determine which parameters cause the most significant changes in the modeled gauge height and flood extent.

Compound flooding scenarios should be designed based on NOAA National Weather Service (NWS) standards. Instead of actual extreme precipitation events, the model should use constant gauge height as the forcing. Also, NOAA NWS suggested using only the Hanalei watershed for compound flood modeling as most of the flooding in Hanalei results from this watershed. NOAA NWS pointed out that the model inaccurately predicts flooding caused by the Wai‘oli Stream (east of the Hanalei River). A higher resolution DEM may solve this problem as it was assumed there is an error in the topography of the Wai‘oli Stream. Burning channels in the Wai‘oli Stream may also help solve this issue, but this adds more complexity and uncertainty to the model.

The extreme sea level scenarios for the compound flood events should be changed. The height of the sea level rise for compound flooding should consider the mean higher high water (MHHW). The model will underestimate the extent of flooding from sea level rise if the MHHW is not added to the sea level rise. The change in sea level between the time of the DEM survey and the year of the sea level rise projection should also be included. The distance between the observed water level at the Nawiliwili 1611400 buoy and Hanalei likely differs. The water level data from Hurricane Iniki could differ from Hanalei Bay. The shape and direction of Hanalei Bay exposes it to different extreme wind or swell events than the towns adjacent to the Nawiliwili 1611400 buoy. A better representation of extreme water levels may be to use return periods from

the Nawiliwili 1611400 buoy. Various combinations of water level and streamflow return periods defined by the buoy and stream gauges can be used for compound flooding scenarios.

Extreme precipitation projections should be considered when evaluating sea level rise flooding. Global models suggest an increase in the magnitude and frequency of extreme precipitation in the future (Chen and Sun, 2021; Thackeray et al., 2022), and Gayte's (2022) study of extreme precipitation trend confirms this is the case for Hanalei. Extreme precipitation projections predict what precipitation events will look like when the sea level rises over the next century. The precipitation projections should use the same timeframe as the expected sea level rise. If extreme precipitation events become more frequent or severe, the streamflow return periods for FEMA flood maps will also change. The flood maps from these projections can be compared to the current FEMA flood maps for further analysis. Incorporating extreme precipitation projections into compound flood models is also a novel area of research that has not been explored much for Hawai'i.

## Appendices

### Appendix A: Duration and Total Number of Floods

The link to download the flood event duration data used to make the map in Figure 1:

<https://uhm.maps.arcgis.com/home/item.html?id=d218934fb6604987bc2fe4b925f7837b>

The link to download the total number of flood events used to make the map in Figure 1:

<https://uhm.maps.arcgis.com/home/item.html?id=6b66b20432bd46ef98e7f747e1c58502>

### Appendix B: Python Scripts

Link to GitHub repository where all the Python scripts and data are saved:

[https://github.com/brianjgorberg/WMS\\_GSSHA\\_Hanalei.git](https://github.com/brianjgorberg/WMS_GSSHA_Hanalei.git)

### Appendix C: Download Link for the GSSHA model of Hanalei Bay

Link to a Figshare repository where all the model files are stored:

[https://figshare.com/articles/dataset/Hanalei\\_Bay\\_GSSHA\\_WMS\\_Software\\_Files\\_for\\_Compound\\_Flood\\_Modeling/26073541](https://figshare.com/articles/dataset/Hanalei_Bay_GSSHA_WMS_Software_Files_for_Compound_Flood_Modeling/26073541)

## Appendix D: Manning's n Roughness Coefficients

**Table 9:** This table contains Manning's n roughness coefficients used within the model.

NOAA C-CAP 2010 Land Use	Manning's N Roughness Coefficients
Impervious Surface	0.02
Developed Open Space	0.045
Cultivated	0.037
Pasture/Hay	0.033
Grassland	0.034
Evergreen Forest	0.047
Scrub/Shrub	0.05
Palustrine Forested Wetland	0.1
Palustrine Scrub/Shrub Wetland	0.048
Palustrine Emergent Wetland	0.045
Unconsolidated Shore	0.04
Bare Land	0.09
Water	0.02

## Appendix E: Metadata of Stream and Rain Gauges

**Table 10:** This table contains the metadata for the stream gauges, rain gauges, and radar data used to build the model.

Type of Data	Name	Source	Start Date	End Date	Latitude	Longitude
Gauge height	USGS 16104200	USGS	5/8/2019	Current	22.17958333	-159.4663889
Streamflow & gauge height	USGS 16103000	USGS	10/1/1990	Current	22.17958333	-159.4663889
Radar	Hourly_radarRF	Huang et al. (2022)	12/31/2015	12/31/2020	na	na
Rain gauge	HI-41	Huang et al. (2022)	2/4/1966	12/31/2020	22.1961	-159.5561
Rain gauge	HI-45	Huang et al. (2022)	4/1/1998	12/31/2020	22.1982002	-159.4951
Rain gauge	KPIH1	Huang et al. (2022)	7/1/1994	12/31/2020	22.1021004	-159.3856
Rain gauge	PRIH1	Huang et al. (2022)	11/23/2014	12/31/2020	22.2113991	-159.4433
Rain gauge	USC00514561	Huang et al. (2022)	2/3/1966	5/8/2018	22.2139	-159.4044
Rain gauge	USC00518165	Huang et al. (2022)	3/18/1965	12/31/2020	22.2181	-159.4828
Rain gauge	USGS_uv220356159281401	Huang et al. (2022)	7/5/2001	12/31/2020	22.0625	-159.4677222
Rain gauge	USGS_uv220427159300201	Huang et al. (2022)	10/1/2007	12/31/2020	22.0708889	-159.4979722
Rain gauge	USGS_uv220443159235601	Huang et al. (2022)	10/1/2007	10/26/2011	22.0756111	-159.3958889
Rain gauge	USGS_uv221101159280801	Huang et al. (2022)	10/1/2007	10/25/2011	22.1795833	-159.4663889
Rain gauge	WUHH1	Huang et al. (2022)	7/1/1994	12/31/2020	22.0660992	-159.396

## Appendix F: Infiltration Parameters

**Table 11:** This table contains the soil parameter values for using the Green and Ampt single-layer infiltration process in the model.

USDA Soil Name	Soil Texture	Hydraulic Conductivity (cm/hr)	Field Capacity (m <sup>3</sup> /m <sup>3</sup> )	Wilting Point (m <sup>3</sup> /m <sup>3</sup> )	Porosity (m <sup>3</sup> /m <sup>3</sup> )	Pore dist. Index (cm/cm)	Initial Soil Moisture	Residual Sat. (m <sup>3</sup> /m <sup>3</sup> )	capillary head (cm)
Rock Outcrop	bedrock	0.079	0.420	0.340	0.666	0.165	0.100	0.090	19.044
Kolokolo	clay loam	2.868	0.269	0.151	0.574	0.242	0.382	0.075	20.880
Riverwash	extremely gravelly sand	33.120	0.460	0.330	0.547	0.694	0.192	0.020	4.950
Hulua	gravelly silty clay loam	9.603	0.329	0.224	0.514	0.177	0.387	0.040	27.300
Alakai	mucky peat	8.517	0.469	0.184	0.770	0.165	0.329	0.090	31.630
Marsh	mucky peat	7.632	0.520	0.360	0.660	0.165	0.329	0.090	31.630
Waialeale	mucky silty clay loam	5.896	0.299	0.133	0.663	0.177	0.387	0.040	27.300
Koolau	silty clay	0.787	0.287	0.167	0.714	0.150	0.404	0.056	29.220
Pooku	silty clay	3.841	0.307	0.222	0.666	0.150	0.404	0.056	29.220
Hanamaulu	silty clay	3.401	0.327	0.231	0.560	0.150	0.404	0.056	29.220
Hihimanu	silty clay loam	2.476	0.311	0.247	0.539	0.177	0.387	0.040	27.300
Hanalei	silty clay loam	2.966	0.321	0.220	0.580	0.177	0.387	0.040	27.300
Rough broken land	silty clay loam	1.660	0.273	0.159	0.737	0.177	0.387	0.040	27.300
Rough mountainous land	silty clay loam	8.729	0.268	0.157	0.601	0.177	0.387	0.040	27.300

**Table 12:** This table contains the soil hydraulic conductivity and thickness values for including the Green and Ampt multi-layer infiltration process in the model. All the other parameters in Table 10 were held constant for each layer.

USDA Soil Name	Soil Texture	Layer 1 Thickness (cm)	Layer 2 Thickness (cm)	Layer 3 Thickness (cm)	Layer 1 Hydraulic Conductivity (cm/hr)	Layer 2 Hydraulic Conductivity (cm/hr)	Layer 3 Hydraulic Conductivity (cm/hr)
Rock Outcrop	bedrock	152.4000	0.1000	0.1000	0.0792	0.0792	0.0792
Kalokolo	clay loam	48.2600	22.8600	81.2800	3.2832	3.2832	2.7756
Riverwash	extremely gravelly sand	15.2400	132.0800	0.1000	32.9400	32.9400	32.9400
Hulua	gravelly silty clay loam	40.6400	5.0800	106.6800	9.6300	0.0792	10.0800
Alakai	mucky peat	20.3200	60.9600	48.2600	27.9216	8.3844	0.8388
Marsh	mucky peat	25.4000	127.0000	0.1000	7.6356	7.6356	7.6356
Waialeale	mucky silty clay loam	17.7800	43.1800	25.4000	8.3232	8.3232	0.0792
Koolau	silty clay	27.9400	53.3400	71.1200	2.8476	0.8388	0.0792
Pooku	silty clay	35.5600	121.9200	0.1000	8.3232	2.7936	2.7936
Hanamaulu	silty clay	27.9400	58.4200	91.4400	8.3232	2.7936	2.7936
Hihimanu	silty clay loam	17.7800	96.5200	68.5800	8.3232	2.7936	1.0152
Hanalei	silty clay loam	30.4800	28.7020	96.5200	2.7756	3.1320	3.3012
Rough broken land	silty clay loam	20.3200	55.8800	76.2000	3.2400	3.2400	0.0792
Rough mountainous land	silty clay loam	12.7000	50.8000	10.1600	10.0800	10.0800	0.0792

## Appendix G: Damage Report of Each Gauge Height Event

**Table 13:** This table contains the social and economic impacts of each gauge height event used in the compound flooding scenarios. The damage report was acquired using data from NCEI (2022).

Gauge Height Scenario (ft)	Actual Peak Height (ft)	Date of Peak	Atmospheric Condition	Damage reported by NCEI (2022)
6	6.02	11/17/2018	cold front (NCEI, 2022)	The Hanalei Bridge was closed during the same week of this event. The cold front brought intense showers and flooding, raising the gauge height to around 6 to 7 feet at its peak.
10	10.01	11/17/2019	cold front (Sears, 2023)	This old cold front combined with an upper-level disturbance to produce heavy showers and thunderstorms. Rainfall affected most of the isles, with flash flooding occurring in Kaua'i and on the Big Island. Kuhio highway was closed near the Hanalei Bridge and impassable as the Wainiha River overflowed its banks at the Twin Bridges in Wainiha. A woman was swept away by the flood waters in that area, but she was rescued by the Kaua'i Fire Department.
14	13.66	11/30/2017	trade winds and upper-level trough (Sears, 2023)	A broad upper trough combined with tropical moisture from the southeast to bring intense showers and isolated thunderstorms to the Big Island and Kaua'i. The northern part of Kaua'i saw flash floods, but no significant property damage or injuries were reported. Kuhio Highway was closed near the Hanalei Bridge.
18	17.65	03/28/2020	upper level low (Sears, 2023)	An atmospheric disturbance brought heavy showers and thunderstorms, especially over the western portion of the Hawaiian Islands. Kuhio Highway was closed near the Hanalei Bridge. At around 04:30 HST, Kuhio Highway closed in Wailua as debris piled up against the bridge. Some homes and businesses in the area were also affected by flood waters.

## Appendix H: USGS 16103000 Stream Gauge’s Streamflow Return Periods

**Table 14:** Streamflow return periods for the USGS 16103000 stream gauges is shown in this table. The USGS StreamStats Tool (2024) provides streamflow values for various flood return periods, with flood events ranging from 2 to 500-year return periods.

USGS Flood Statistic	Return period (yrs)	Streamflow (ft <sup>3</sup> /sec)
50% AEP flood	2	15900
20% AEP flood	5	22200
10% AEP flood	10	26200
4% AEP flood	25	31100
1% AEP flood	100	38000
0.5% AEP flood	200	414300
0.2% AEP flood	500	45600

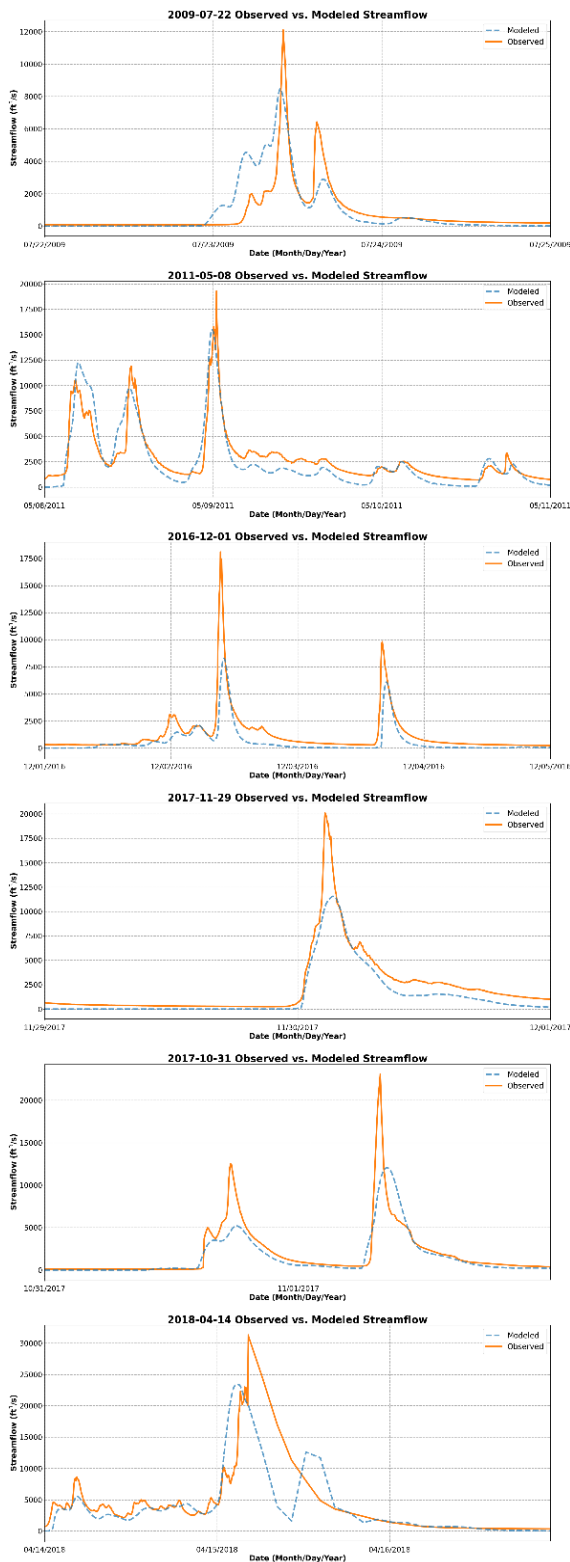
## Appendix I: NSE Values from Calibration Simulations

**Table 15:** This table contains the NSE values for each of the six streamflow events used for calibration. The three Evergreen Forest Manning’s n roughness parameters that were tested include 0.11, 0.047, and 0.4.

Simulation Date	Manning's N Roughness Parameter and NSE values		
	0.11	0.047	0.4
7/22/2009	0.56	0.56	0.67
5/8/2011	0.76	0.76	0.22
12/1/2016	0.3	0.56	0.08
10/31/2017	0.58	0.67	-0.22
11/29/2017	0.74	0.83	0.21
4/14/2018	0.51	0.42	0.69

# Appendix J: Graphs of Validation and Calibration Simulations

## CALIBRATION GRAPHS



## VALIDATION GRAPHS

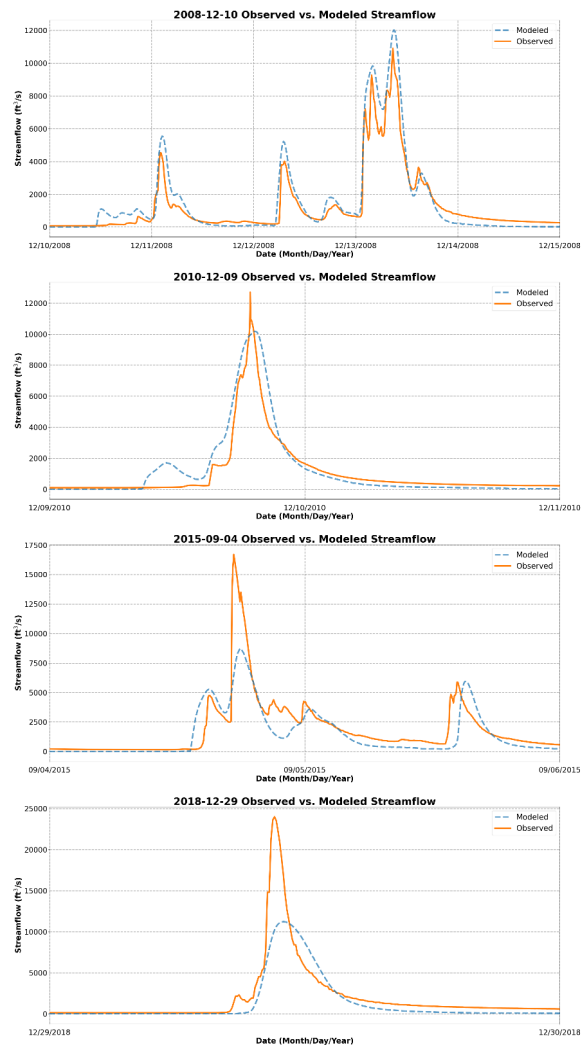


**Figure 16:** The column of plots on the left displays the modeled and observed streamflow from calibration events. The column of plots to the right shows the events used for validation. A roughness value of 0.047 for the 'Evergreen Forest' land use was used for each simulation that is plotted.

Appendix K: Compound Flood Maps

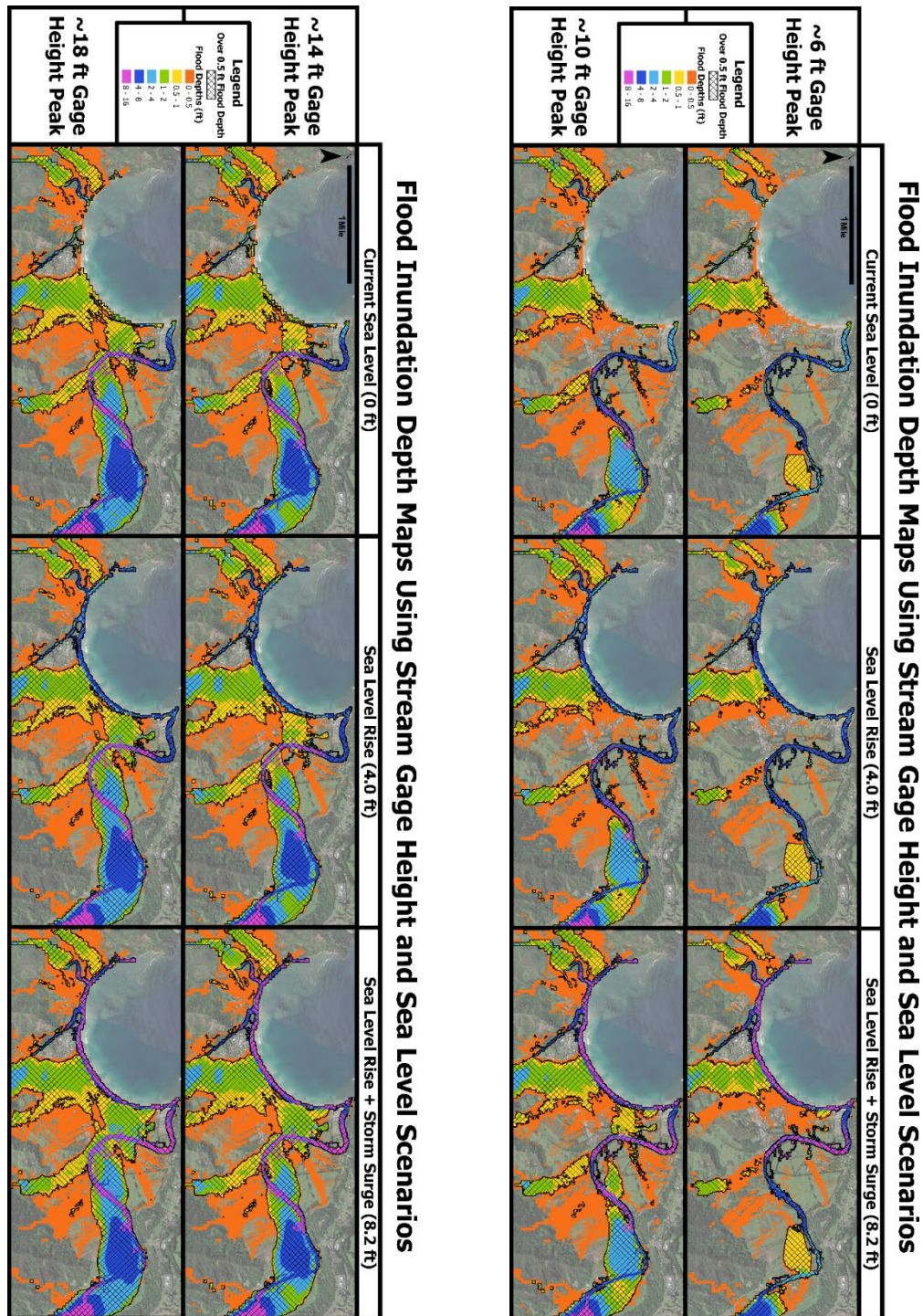


**Figure 17:** The twelve maximum flood maps from the compound flooding scenarios are shown. The maps should not be used for planning, mitigation, or engineering purposes yet.

The link to download the flood maps:

<https://uhm.maps.arcgis.com/home/item.html?id=7623872db5c64bb2ac96b1cbf7140e55>

## References

- Afshari, S., Feng, D., Omranian, E., & Zarzar, C. (2016). Relative Sensitivity of Flood Inundation Extent by Different Physical and Semi empirical Models. <http://dx.doi.org/10.4211/technical.20161019>
- AghaKouchak, A., Chiang, F., Huning, L. S., Love, C. A., Mallakpour, I., Mazdiyasn, O., Moftakhari, H., Papalexiou, S.M., Ragno, E., & Sadegh, M. (2020). Climate extremes and compound hazards in a warming world. *Annual Review of Earth and Planetary Sciences*, 48(1), 519–548. <https://doi.org/10.1146/annurev-earth-071719-055228>
- Ahmadisharaf, E., Camacho, R. A., Zhang, H. X., Hantush, M. M., & Mohamoud, Y. M. (2019). Calibration and Validation of Watershed Models and Advances in Uncertainty Analysis in TMDL Studies. *Journal of Hydrologic Engineering*, 24(7). [https://doi.org/10.1061/\(asce\)he.1943-5584.0001794](https://doi.org/10.1061/(asce)he.1943-5584.0001794)
- Anderson T. R., Fletcher, C. H., Barbee, M. M., Romine, B. M., Lemmo, S., & Delevaux, J. M. S. (2018). Modeling multiple sea level rise stresses reveals up to twice the land at risk compared to strictly passive flooding methods. *Scientific Reports*, 8(1). <https://doi.org/10.1038/s41598-018-32658-x>
- Bezore, R. (2014). A Comparative Study of Passive versus Dynamic Sea-Level Rise Inundation Models for the Island of Kauai. Master's Thesis. University of California Santa Cruz. accessed on 08/01/2024 at URL <https://www.proquest.com/dissertationtheses/comparative-study-passive-versus-dynamic-sea/docview/1620842735/se-2>
- Brakenridge, G. R. & Kettner, A. J. (2018). DFO Flood Event 4601. Dartmouth Flood Observatory, University of Colorado, Boulder, Colorado, USA. accessed on 08/01/2024 at URL <https://floodobservatory.colorado.edu/Events/2018USA4601/2018USA4601.html>
- Brendel, C. E., Dymond, R. L., & Aguilar, M. F. (2021). Modeling Storm Sewer Networks and Urban Flooding in Roanoke, Virginia, with SWMM and GSSHA. *Journal of Hydrologic Engineering*, 26(1). [https://doi.org/10.1061/\(asce\)he.1943-5584.0002021](https://doi.org/10.1061/(asce)he.1943-5584.0002021)
- Brooks, R. H., & Corey, A. T. (1963). Hydraulic Properties of Porous Media. *Hydrology Paper*, 3. accessed on 08/01/2024 at URL [https://mountainscholar.org/bitstream/handle/10217/197982/CERF\\_63\\_24.pdf](https://mountainscholar.org/bitstream/handle/10217/197982/CERF_63_24.pdf)
- Chen, H., & Sun, J. (2021). Significant increase of the global population exposure to increased precipitation extremes in the future. *Earth's Future*, 9, <https://doi.org/10.1029/2020EF001941>

- Cheng, C. L., Fares, A., El-Kadi, A., Abbas, F., & Robotham, M. (2007). Evaluating the Performance of AnnAGNPS and N-SPECT for Tropical Conditions. Master's thesis. University of Hawaii at Manoa, Honolulu, USA. accessed on 08/01/2024 at URL <https://scholarspace.manoa.hawaii.edu/items/197b1169-3328-424a-bdff-811c118baba8>
- Chu, P-S., Zhao, X., Ruan, Y., & Grubbs, M. (2009). Extreme rainfall events in the Hawaiian Islands. *Journal of Applied Meteorology and Climatology*, 48(3), 502–516. <https://doi.org/10.1175/2008JAMC1829.1>
- Corrigan, T. J., & Businger, S. (2022). The Anatomy of a Series of Cloud Bursts that Eclipsed the U.S. Rainfall Record. *Monthly Weather Review*, 150(4), 753–773. <https://doi.org/10.1175/MWR-D-21-0028.1>
- Costabile, P., Costanzo, C., De Lorenzo, G., & Macchione, F. (2020). Is local flood hazard assessment in urban areas significantly influenced by the physical complexity of the hydrodynamic inundation model?. *Journal of Hydrology*, 580. <https://doi.org/10.1016/j.jhydrol.2019.124231>
- Downer, C. W., & Ogden, F. L. (2006). System-Wide Water Resources Program Gridded Surface Subsurface Hydrologic Analysis (GSSHA) User's Manual Version 1.43 for Watershed Modeling System 6.1. accessed on 08/01/2024 at URL <https://apps.dtic.mil/sti/tr/pdf/ADA455335.pdf>
- Fares, A. (2008). Overview of the hydrological modeling of small coastal watersheds on tropical islands. *Coastal Watershed Management*. accessed on 08/01/2024 at URL <https://api.semanticscholar.org/CorpusID:199401684>
- Fares, A., Awal, R., Michaud, J., Chu, P-S., Fares, S., Kodama, K., & Rosener, M. (2014). Rainfall-runoff modeling in a flashy tropical watershed using the distributed HL-RDHM model. *Journal of Hydrology*, 519, 3436–3447. <https://doi.org/10.1016/j.jhydrol.2014.09.042>
- FEMA (2010). Flood Insurance Study: Kaua'i County, Volume 1 of 2. Federal Emergency Management Agency: Washington, DC. accessed on 08/01/2024 at URL <https://dlnreng.Hawai'i.gov/nfip/wp-content/uploads/sites/11/2018/01/150002V001C-11262010.pdf>
- FEMA (2022). Hydrologic Numerical Models Meeting the Minimum Requirement of National Flood Insurance Program. *FEMA*. accessed on 08/01/2024 at URL <https://www.fema.gov/flood-maps/products-tools/numerical-models/hydrologic>

- Feng, D., Tan, Z., Engwirda, D., Liao, C., Xu, D., Bisht, G., Zhou, T., Li, H.-Y., & Leung, L. R. (2022). Investigating coastal backwater effects and flooding in the coastal zone using a global river transport model on an unstructured mesh. *Hydrology and Earth System Sciences*, 26(21), 5473–5491. <https://doi.org/10.5194/hess-26-5473-2022>
- Feng, D., Tan, Z., Xu, D., & Leung, L. R. (2023). Understanding the compound flood risk along the coast of the contiguous United States. *Hydrology and Earth System Sciences*, 27(21), 3911–3934, <https://doi.org/10.5194/hess-27-3911-2023>, 2023.
- Fereshtehpour, M., & Karamouz, M. (2018). DEM resolution effects on coastal flood vulnerability assessment: Deterministic and probabilistic approach. *Water Resources Research*, 54, 4965–4982. <https://doi.org/10.1029/2017WR022318>
- Field, M. E., Berg, C. S., & Cochran, S. A. (2007). Science and Management in the Hanalei Watershed: A Trans-Disciplinary Approach Proceedings from the Hanalei Watershed Workshop. USGS Open-File Report 2007-1219, 87 p. accessed on 08/01/2024 at URL <https://www.academia.edu/download/30726720/Science-Management-in-Hanalei-Watershed.pdf#page=45>
- Fortini, L. B., Leopold, C., Perkins, K., Chadwick, O., Yelenik, S., Jacobi, J., Ena, K., Ii, B., Gregg, M., & Rosa, S. (2020). Local to landscape-level controls of water fluxes through Hawaiian forests: effects of invasive animals and plants on soil infiltration capacity across substrate and moisture gradients. accessed on 08/01/2024 at URL <http://pubs.usgs.gov/circ/1367/>
- Frazier, A., & Giambelluca, T. (2017). Spatial trend analysis of Hawaiian rainfall from 1920 to 2012. *International Journal of Climatology*, 37(5), 2522–2531. <https://doi.org/10.1002/joc.4862>
- Fuddy, L. J. & Abercrombie, N. (2011). Total Maximum Daily Loads for the Hanalei Bay Watershed, PHASE 2-Embayment. accessed on 08/01/2024 at URL [https://health.hawaii.gov/cwb/files/2013/05/Integrated\\_HanaleiPhase2.pdf](https://health.hawaii.gov/cwb/files/2013/05/Integrated_HanaleiPhase2.pdf)
- Furl, C., Ghebreyesus, D., & Sharif, H. O. (2018). Assessment of the performance of satellite-based precipitation products for flood events across diverse spatial scales using the GSSHA modeling system. *Geosciences (Switzerland)*, 8(6). <https://doi.org/10.3390/geosciences8060191>

- Garcia, E. S. & Loáiciga, H. A. (2014). Sea-level rise and flooding in coastal riverine flood plains. *Hydrological Sciences Journal*, 59(1), 204-220.  
<https://doi.org/10.1080/02626667.2013.798660>
- Garrote, J., Díez-Herrero, A., Génova, M., Bodoque, J. M., Perucha, M. A., & Mayer, P. L. (2018). Improving flood maps in ungauged fluvial basins with dendrogeomorphological data. An example from the caldera de Taburiente national park (Canary Islands, Spain). *Geosciences (Switzerland)*, 8(8). <https://doi.org/10.3390/geosciences8080300>
- Gayte, M., Tsang, Y., Giambelluca, T., & Chu, P. S. (2022). Characterizing rainfall regime changes and estimating the timing of high streamflow events across the five main hawaiian islands. Master's thesis. University of Hawaii at Manoa, Honolulu, USA.  
accessed on 08/01/2024 at URL  
<https://scholarspace.manoa.hawaii.edu/server/api/core/bitstreams/c0e89fd0-a1ba-445a-9169-1b007b6b407c/content>
- Giambelluca, T. W., Chen, Q., Frazier, A. G., Price, J. P., Chen, Y. L., Chu, P-S., Eischeid, J.K., & Delparte, D.M. (2013). Online Rainfall Atlas of Hawai'i. *Bulletin of American Meteorology Society*, 94, 313-316. <https://doi.org/10.1175/BAMS-D-11-00228.1>
- Gupta, H. V., Kling, H., Yilmaz, K. K., & Martinez, G. F. (2009). Decomposition of the mean squared error and NSE performance criteria: Implications for improving hydrological modeling, *Journal of Hydrology*, 377(1-2), 80–91.  
<https://doi.org/10.1016/j.jhydrol.2009.08.003>
- Hagedorn, B., & El-Kadi, A. (2009). Evaluation of FLO-2D runoff and sediment loading models in tropical humid to semi-arid catchments of Hawaii. AGU Fall Meeting Abstracts.  
accessed on 08/01/2024 at URL  
[https://www.researchgate.net/publication/253778780\\_Evaluation\\_of\\_FLO-2D\\_runoff\\_and\\_sediment\\_loading\\_models\\_in\\_tropical\\_humid\\_to\\_semi-arid\\_catchments\\_of\\_Hawaii](https://www.researchgate.net/publication/253778780_Evaluation_of_FLO-2D_runoff_and_sediment_loading_models_in_tropical_humid_to_semi-arid_catchments_of_Hawaii)
- Hall, J. W., Tarantola, S., Bates, P. D., & Horritt, M. S. (2005). Distributed sensitivity analysis of flood inundation model calibration. *Journal of Hydraulic Engineering*, 131(2).  
[https://doi.org/10.1061/\(ASCE\)0733-9429\(2005\)131:2\(117\)](https://doi.org/10.1061/(ASCE)0733-9429(2005)131:2(117))
- Hawai'i DLNR DAR. (2020). Surface water hydrologic unit boundaries for hydrologic water catchment for the main Hawaiian Islands (excluding Kahoolawe) - DAR's version.  
Retrieved from [https://files.hawaii.gov/dbedt/op/gis/data/watersheds\\_dar.shp.zip](https://files.hawaii.gov/dbedt/op/gis/data/watersheds_dar.shp.zip)

- Hawai‘i Statewide GIS Program. (2021). Hawaii DTM. Retrieved from <https://prod-histategis.opendata.arcgis.com/datasets/HiStateGIS::hawaii-dtm/explore?location=20.468962%2C-157.496600%2C6.57>
- Hawai‘i Statewide GIS Program. (2024). Parcels - Hawai‘i Statewide. accessed on 08/01/2024 at URL [https://geoportal.hawaii.gov/datasets/579b8dcb7a8e44c1af201e1b3cdf655f\\_25/explore?location=20.533920%2C-157.641050%2C7.32](https://geoportal.hawaii.gov/datasets/579b8dcb7a8e44c1af201e1b3cdf655f_25/explore?location=20.533920%2C-157.641050%2C7.32)
- Hendry, A., Haigh, I. D., Nicholls, R. J., Winter, H., Neal, R., Wahl, T., Joly-Laugel, A., & Darby, S. E. (2023). Assessing the characteristics and drivers of compound flooding events around the UK coast. *Hydrology and Earth System Sciences*, 23, 3117–3139. <https://doi.org/10.5194/hess-23-3117-2019>
- Huang, Y-F., Gayte, M., Tsang, Y., Longman, R. J., Nugent, A. D., Kodama, K., Lucas, M. P., Giambelluca, T. W. (2022). Hourly rainfall data from rain gauge networks and weather radar up to 2020 across the Hawaiian Islands. figshare. Collection. <https://doi.org/10.6084/m9.figshare.c.5779532.v1>
- Huang, Y-F., Tsang, Y., Strauch, A. M., & Clilverd, H. M. (2021). Shifting magnitude and timing of streamflow extremes and the relationship with rainfall across the Hawaiian Islands. *Journal of Hydrology*, 600. <https://doi.org/10.1016/j.jhydrol.2021.126424>
- HWH and SRGI. (2023). Hanalei Watershed Flood Mitigation Study. accessed on 08/01/2024 at URL <https://www.hanaleiwatershedhui.org/flood-study>
- Kalyanapu, A., Burian, S., & Mcpherson, T. (2009). Effect of land use-based surface roughness on hydrologic model output. *Journal of Spatial Hydrology*, 9, 51-71. Retrieved from [https://www.researchgate.net/publication/264933073\\_Effect\\_of\\_land\\_use-based\\_surface\\_roughness\\_on\\_hydrologic\\_model\\_output](https://www.researchgate.net/publication/264933073_Effect_of_land_use-based_surface_roughness_on_hydrologic_model_output)
- Kauai Climate Adaptation Plan. (2022). Open House Series #1 Summary Report. Kauai Climate Adaptation Plan. accessed on 08/01/2024 at URL [https://kauaiadaptation.com/wp-content/uploads/2022/07/KCAP\\_OpenHouse1\\_FINALSummary\\_22\\_0707.pdf](https://kauaiadaptation.com/wp-content/uploads/2022/07/KCAP_OpenHouse1_FINALSummary_22_0707.pdf)
- Knoben, W. J. M., Freer, J. E., & Woods, R. A. (2019). Technical note: Inherent benchmark or not? Comparing Nash–Sutcliffe and Kling–Gupta efficiency scores. *Hydrology and Earth System Science*, 23, 4323–4331. <https://doi.org/10.5194/hess-23-4323-2019>

- Laramee, L., Bradley, R., Amy, W., Fletcher, C., Habel, S., Budge, J., Lee, C., & Ho, A. (2022). Sea Level Rise Vulnerability and Adaptation Report prepared by the State of Hawaii Department of Land and Natural Resources, Office of Conservation and Coastal Lands. accessed on 08/01/2024 at URL <https://climate.hawaii.gov/wp-content/uploads/2023/01/OCCL23-Sea-Level-Rise-Report-FY22.pdf>
- Liu, Z., Merwade, V., & Jafarzadegan, K. (2019). Investigating the role of model structure and surface roughness in generating flood inundation extents using one- and two-dimensional hydraulic models. *Journal of Flood Risk Management*, 12(1). <https://doi.org/10.1111/jfr3.12347>
- Manrique, S. A., Harmsen, E. W., Khanbilvardi, R. M., & González, J. E. (2021). Flood impacts on critical infrastructure in a coastal floodplain in western Puerto Rico during hurricane María. *Hydrology*, 8(3). <https://doi.org/10.3390/hydrology8030104>
- Mathews, L. (2018). Record-Breaking Rains Devastated Kauai's Hanalei Bay This Weekend, 16 Apr. 2018. accessed on 08/01/2024 at URL [www.townandcountrymag.com/leisure/travel-guide/a19828954/hanalei-kauai-hawaii-flash-flooding/](http://www.townandcountrymag.com/leisure/travel-guide/a19828954/hanalei-kauai-hawaii-flash-flooding/)
- Mattocks, C. & Forbes, C. (2008). A real-time, event-triggered storm surge forecasting system for the state of North Carolina. *Ocean Modelling*, 25(3–4), 95–119. <https://doi.org/10.1016/j.ocemod.2008.06.008>
- Medeiros, S. C., Hagen, S. C., & Wieshampel, J. F. (2012). Comparison of floodplain surface roughness parameters derived from land cover data and field measurements. *Journal of Hydrology*, 452–453, 139–149. <https://doi.org/10.1016/j.jhydrol.2012.05.043>
- Mirchi, A., Watkins, D., & Madani, K. (2009). Modeling for Watershed Planning, Management, and Decision Making. *Watersheds: Management, Restoration and Environmental Impact*. Retrieved from [https://www.researchgate.net/publication/285210813\\_Modeling\\_for\\_watershed\\_planning\\_management\\_and\\_decision\\_making](https://www.researchgate.net/publication/285210813_Modeling_for_watershed_planning_management_and_decision_making)
- Mitu, M. F., Sofia, G., Shen, X., & Anagnostou, E. N. (2023). Assessing the compound flood risk in coastal areas: Framework formulation and demonstration. *Journal of Hydrology*, 626. <https://doi.org/10.1016/j.jhydrol.2023.130278>
- Moriassi, D. N., Arnold, J. G., Van Liew, M. W., Bingner, R. L., Harmel, R. D., & Veith, T. L. (2007). Model evaluation guidelines for systematic quantification of accuracy in

- watershed simulations. *Transactions of the ASABE*, 50(3), 885–900.  
<https://doi.org/10.13031/2013.23153>
- Nadiatul Adilah, A. A. G., & Hannani, H. (2021). Comparison of Methods to Estimate Missing Rainfall Data for Short Term Period at UMP Gampang. *IOP Conference Series: Earth and Environmental Science*, 682(1). <https://doi.org/10.1088/1755-1315/682/1/012027>
- Nash, J. E., & Sutcliffe, J. V. (1970). River flow forecasting through conceptual models: Part 1. A discussion of principles. *Journal of Hydrology*, 10(3), 282–290.  
[https://doi.org/10.1016/0022-1694\(70\)90255-6](https://doi.org/10.1016/0022-1694(70)90255-6)
- NCEI. (2022). Storm Data and Unusual Weather Phenomena With Late Reports and Corrections. National Centers for Environmental Information website, accessed on 10/01/2022 at URL <https://www.ncdc.noaa.gov/stormevents/>
- NOAA C-CAP (2010). 2010 C-CAP Land Cover, Kauai, Hawaii (published 20130528). accessed on 10/20/2022 at URL <https://chs.coast.noaa.gov/htdata/raster1/landcover/bulkdownload/hires/hi/>
- NOAA Sea Level Projection. (2024). Nawiliwili Bay, Kauai Island Projected Sea Level Rise Under Different SSP Scenarios. Accessed on 07/02/2024 at URL [https://sealevel.nasa.gov/ipcc-ar6-sea-level-projection-tool?psmsl\\_id=756&data\\_layer=scenario](https://sealevel.nasa.gov/ipcc-ar6-sea-level-projection-tool?psmsl_id=756&data_layer=scenario)
- Ogden, F. L. (2016). Evidence of equilibrium peak runoff rates in steep tropical terrain on the island of Dominica during Tropical Storm Erika. *Journal of Hydrology*, 542, 35–46.  
<https://doi.org/10.1016/j.jhydrol.2016.08.041>
- Paoa, N., Fletcher, C. H., Anderson, T. R., Coffman, M., & Habel, S. (2023). Probabilistic sea level rise flood projections using a localized ocean reference surface. *Scientific Reports*, 13(1). <https://doi.org/10.1038/s41598-023-29297-2>
- Petterson, J. S., & Glazier, E. W., Kittinger, J., Stevens, J., & Scarl, R. (2012). Fishing, Seafood, and Community Research in the Main Hawaiian Islands: A Case Study of Hanalei Bay, Kaua'i. accessed on 08/01/2024 at URL <https://repository.library.noaa.gov/view/noaa/965>
- Pradhan, N. R., Downer, C. W., Sinclair, S. N., & Lahatte, C. (2019). Simulation of coastal storm surge and rainfall flooding scenarios at Camp Lejeune with GSSHA. *ERDC/CHL*

- CHETN-I-96*. accessed on 08/01/2024 at URL  
<https://erdclibrary.erdc.dren.mil/items/686dd4df-707f-4237-ae90-90a2156df4be>
- Rao, A. R., & Han, J. (1987). Analysis of objective functions used in urban runoff models. *Advanced Water Resources*, 10, 205–211. [https://doi.org/10.1016/0309-1708\(87\)90030-3](https://doi.org/10.1016/0309-1708(87)90030-3)
- Rawls, W. J., Brakensiek, D. L., & Miller, N. (1983) Green-Ampt infiltration parameters from soil data. *Journal of Hydraulic Engineering (ASCE)*, 109.  
[https://doi.org/10.1061/\(ASCE\)0733-9429\(1983\)109:1\(62\)](https://doi.org/10.1061/(ASCE)0733-9429(1983)109:1(62))
- Safeeq, M., & Fares, A. (2012). Hydrologic response of a Hawaiian watershed to future climate change scenarios. *Hydrological Processes*, 26(18), 2745–2764.  
<https://doi.org/10.1002/hyp.8328>
- Sangsefidi, Y., Bagheri, K., Davani, H., & Merrifield, M. (2023). Data analysis and integrated modeling of compound flooding impacts on coastal drainage infrastructure under a changing climate. *Journal of Hydrology*, 616.  
<https://doi.org/10.1016/j.jhydrol.2022.128823>
- Schilt, R. A. (1980). Archaeological Investigations in Specified Areas of the Hanalei Wildlife Refuge, Hanalei Valley, Kaua‘i. Technical report prepared for United States Fish and Wildlife Service. Department of Anthropology, Bernice P. Bishop Museum. Honolulu. . accessed on 08/01/2024 at URL <https://core.tdar.org/document/358576/archaeological-investigations-in-specified-areas-of-the-hanalei-wildlife-refuge-hanalei-valley-kauai>
- Sears, M. J., Nugent, A. D., Tsang, Y., & Chu, P-S. (2023). Flooding from the Ground Up: An Analysis of Rain and River Behavior on the North Shore of Kaua‘i. ProQuest Dissertations & Theses. . accessed on 08/01/2024 at URL  
<http://eres.library.manoa.hawaii.edu/login?url=https://www.proquest.com/dissertations-theses/flooding-ground-up-analysis-rain-river-behavior/docview/2835406575/se-2?accountid=27140>
- Servat, E., & Dezetter, A. (1991). Selection of calibration objective functions in the context of rainfall-runoff modeling in a Sudanese savannah area. *Hydrological Sciences Journal*, 36(4), 307–330. <https://doi.org/10.1080/02626669109492517>
- Shade, P. (1996). Water budget for the island of Kauai. USGS water resources investigations report 95-4128. accessed on 08/01/2024 at URL  
<http://pubs.er.usgs.gov/publication/wri954128>

- Singh, V. P., & Woolhiser, D. A. (2002). Mathematical modeling of watershed hydrology. *Journal of Hydrological Engineering*, 7, 270–292. [https://doi.org/10.1061/\(ASCE\)1084-0699\(2002\)7:4\(270\)](https://doi.org/10.1061/(ASCE)1084-0699(2002)7:4(270))
- Sith, R., & Nadaoka, K. (2017). Comparison of SWAT and GSSHA for high time resolution prediction of stream flow and sediment concentration in a small agricultural watershed. *Hydrology*, 4(2). <https://doi.org/10.3390/hydrology4020027>
- Sorooshian, S., Duan, Q. Y., & Gupta, V. K. (1993). Calibration of rainfall runoff models—Application of global optimization to the Sacramento Soil-Moisture Accounting Model. *Water Resource Research*, 29, 1185–1194. <https://doi.org/10.1029/92WR02617>
- Sun, H., Zhang, X., Ruan, X., Jiang, H., Shou, W. (2024). Mapping compound flooding risks for urban resilience in coastal zones: A comprehensive methodological review. *Remote Sensing*, 16(2), 350. <https://doi.org/10.3390/rs16020350>
- Sweet, W. V., Hamlington, B. D., Kopp, R. E., Weaver, C. P., Barnard, P. L., Bekaert, D., Brooks, W., Craghan, M., Dusek, G., Frederikse, T., Garner, G., Genz, A. S., Krasting, J. P., Larour, E., Marcy, D., Marra, J. J., Obeysekera, J., Osler, M., Pendleton, M., Roman, D., Schmeid, L., Veatch, W., White, K. D., & Zuzak, C. (2022). Global and regional sea level rise scenarios for the United States: updated mean projections and extreme water level probabilities along US coastlines. USGS Publications Warehouse. . accessed on 08/01/2024 at URL <https://pubs.usgs.gov/publication/70229139>
- Taylor, B. (2018). “X.Com.” *X (Formerly Twitter)*, 15 Apr. 2018. Retrieved from [x.com/eminiwatch/status/985589457163177984](https://x.com/eminiwatch/status/985589457163177984)
- Thackeray, C. W., Hall, A., Norris, J., Chen, D.. (2022). Constraining the increased frequency of global precipitation extremes under warming. *Nature Climate Change*, 12, 441–448. <https://doi.org/10.1038/s41558-022-01329-1>
- Thompson, P. R., Widlansky, M. J., Merrifield, M. A., Becker, J. M., & Marra, J. J. (2019). A Statistical Model for Frequency of Coastal Flooding in Honolulu, Hawaii, During the 21st Century. *Journal of Geophysical Research: Oceans*, 124(4), 2787–2802. <https://doi.org/10.1029/2018JC014741>
- Titterington, J., Squibbs, G. , Digman, C., Allitt, R., Osborne, M., Eccleston, P., & Wisdich, A. (2017). Code of practice for the hydraulic modeling of urban drainage systems. *London: Chartered Institution of Water and Environmental Management*. accessed on 08/01/2024 at URL

<https://www.ciwem.org/assets/pdf/Special%20Interest%20Groups/Urban%20Drainage%20Group/Code%20of%20Practice%20for%20the%20Hydraulic%20Modelling%20of%20Ur.pdf>

Tolson, B. A., & Shoemaker, C. A. (2007). Dynamically dimensioned search algorithm for computationally efficient watershed model calibration. *Water Resources Research*, 43(1). <https://doi.org/10.1029/2005WR004723>

USACE (2020). Ala Wai Flood Risk Management Project Honolulu, Hawaii. *Engineering Documentation Report*. accessed on 08/01/2024 at URL [https://www.poh.usace.army.mil/Portals/10/docs/Ala%20Wai%20FRM/Ala%20Wai%20EDR%20Signed.pdf?ver=QaO0uUE\\_k-lrwz1McPsl4w%3d%3d](https://www.poh.usace.army.mil/Portals/10/docs/Ala%20Wai%20FRM/Ala%20Wai%20EDR%20Signed.pdf?ver=QaO0uUE_k-lrwz1McPsl4w%3d%3d)

USDA (2019). U.S. Department of Agriculture, Natural Resources Conservation Service Geographic (SSURGO) soils database for Island of Kauai, Hawaii (published 20190916). Accessed 10/20/2022 at URL <https://websoilsurvey.sc.egov.usda.gov/>

USGS (2013). U.S. Geological Survey 13 arc-second n23w160 1 x 1 degree (published 20130101), accessed 10/20/2022 at URL [https://prd-tnm.s3.amazonaws.com/StagedProducts/Elevation/1/TIFF/historical/n23w160/USGS\\_1\\_n23w160\\_20130911.tif](https://prd-tnm.s3.amazonaws.com/StagedProducts/Elevation/1/TIFF/historical/n23w160/USGS_1_n23w160_20130911.tif)

USGS StreamStats Tool. (2024). USGS StreamStats Gage Page for Station Number 16103000. Retrieved from <https://streamstats.usgs.gov/ss/?gage=16103000&tab=info>

Van de Sande, B., Lansen, J., Hoyng, C. (2012). Sensitivity of Coastal Flood Risk Assessments to Digital Elevation Models. *Water*, 4(3), 568-579. <https://doi.org/10.3390/w4030568>

Wahl, T., Jain, S., Bender, J., Meyers, S. D., & Luther, M. E. (2015). Increasing risk of compound flooding from storm surge and rainfall for major US cities. *Nature Climate Change*, 5, 1093–1097. <https://doi.org/10.1038/nclimate2736>

Wahlstrom, E., Loague, K., & Kyriakidis, P. C. (1999). Hydrologic Response: Kaho'olawe, Hawaii. *Journal of Environmental Quality*, 28 (2), 481–492. <https://doi.org/10.2134/jeq1999.00472425002800020013x>

White, K. L., & Chaubey, I. (2005). Sensitivity Analysis, Calibration and Validation for a Multisite and Multivariable SWAT Model. *Journal of American Water Resources Association*, 41, 1077-1089. <http://dx.doi.org/10.1111/j.1752-1688.2005.tb03786.x>

Xu, K., Wang, C., & Bin, L. (2023). Compound flood models in coastal areas: a review of methods and uncertainty analysis. *Natural Hazards*, *116*, 469–496.  
<https://doi.org/10.1007/s11069-022-05683-3>